

以报考高孟秋导师为例

首都医科大学附属北京胸科医院

2025级博士申请考核材料

考生姓名：某某某

报考导师：高孟秋

报考专业：内科学

硕士毕业院校：信息科技大学

目录

一.材料 1.博士研究生报名登记表.....	3
二.材料 2.身份证正反面复印后扫描件	9
三.材料 3.本科和硕士学历、学位证书, 应届生在读证明	11
四.材料 4.本科和硕士成绩单	15
五.材料 5.思想政治情况表	18
六.材料 6.英语水平成绩单或证明	20
七.材料 8.取得的科研成果	23
八.材料 9.其他科研能力和综合水平的证明材料	53
九.材料 11.攻读博士学位的研究计划书	56
十.材料 12.其他材料	65

一.材料 1.报名信息简表

博士学位研究生网上报名信息简表

报名号		8711200000				
基本信息	姓名	贾	姓名拼音	jiyyyyyy		
	证件类型	(01)居民身份证	证件号码	13100000000000		
	出生日期	1900000	性别	(2)女		
	婚姻状况	(2)已婚	现役军人	(0)非现役军人		
	民族	(01)汉族	政治面貌	(01)中国共产党党员		
	出生地	(131082)中国				
	籍贯地	(131082)中国				
	户口所在地	(110101)北京xxx				
	档案所在地	(110112)北京xxxx				
	档案所在单位	北京xxxx				
	档案所在单位地址	北xxxxx				
	档案所在单位邮政编码	101149				
	考生来源	(32)其他专业技术人员				
	现学习工作单位性质	(24)医疗卫生单位				
	现学习工作单位	胸xxxxxxxx				

学习与工作经历	何时何地何原因 受过何种奖励或 处分	无		
	发表的主要学术 论文和著作	-		
	起止年月	学习与工作经历(高中毕业后起)		任何职务
	2022年6月至今	高中写起，无断档		无
家庭主要成员	姓名	与本人关系	在何单位工作或学习、任何职务	联系电话
	XXXX	XX	北XXXXXX	无

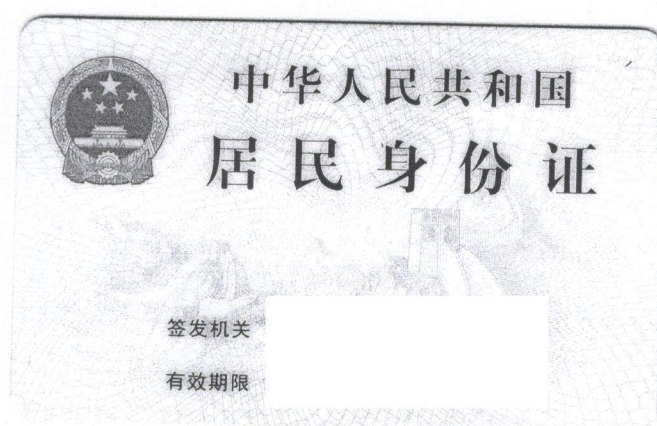
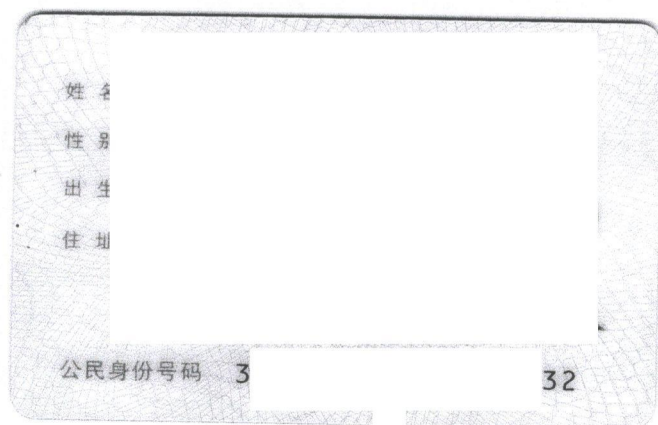
学历学位信息	最后学位	(310)医学硕士		
	最后学历	(2)硕士研究生		
	取得本科学历的学习形式	全日制		
	本科毕业单位所在省市	北京市		
	本科毕业单位	xxx		
	本科毕业专业	xxx		
	本科毕业年月	xxxxxx	本科毕业证书编号	xxxxxxxx
	学士学位单位所在省市	xxx		
	获学士学位单位	xxxx		
	学士学位专业	xxxx		
	获学士学位年月	xxxx	学士学位证书编号	xxxx
	硕士毕业单位所在省市	(11)北京市		
	硕士毕业单位	(87112)北xxxxxx		
	硕士毕业专业	(100201)内科学		
	硕士毕业年月	2023-03	硕士毕业证书编号	1234
	在校生注册学号	仅在校生填写		
	获硕士学位方式	(1)学历教育		
	硕士学位单位所在省市	(11)北京市		
	获硕士学位单位	(87112)北xxxx		
	硕士学位专业	(100201)内科学		
获硕士学位年月	2023-04	硕士学位证书编号	1xxxx234	
联系信息	通信地址	北关大街9号		
	邮政编码	101149		
	固定电话	13xxxxxxxx87	移动电话	13xxxxxxxx87
	电子信箱	yuxxxxxxxx@163.com		

报考信息	报考单位	(87112)北京市结核病胸部肿瘤研究所		
	报考院系所	(000)不区分院系所		
	报考专业	(100201)内科学		
	报考研究方向	(07)肿瘤核医学，心血管核医学，神经核医学	报考学习方式	(1)全日制
	报考博导姓名	李翔		
	考试方式	(99)申请考核	专项计划	(0)无
	报考类别	(11)非定向就业		
	定向就业单位所在地			
	定向就业单位			
	外国语	(1001)申请考核英语笔试		
	业务课一	(2002)申请考核理论笔试-内科学		
	业务课二	(3001)申请考核应用能力笔试		
备用信息	备用信息			
	备用信息1			
	备用信息2			
	备用信息3			
其他	报名时间	2023-10-24 15:25:46	最后修改时间	
	考生登录用户名	13720054687	报名信息简表生成时间	2023-10-25 11:17:16

本人自述(包括政治表现、外语水平、业务和科研能力，可另附页说明)
<div>自行填写</div>
考生所在单位人事部门意见(需注明同意报考何种类别的博士生：定向就业、非定向就业)
<div>电子版无需盖章签名，最迟面试前需提交盖章签字版</div> <div> 负责人签名： 年 月 日 单位盖章 年 月 日 </div>
<div> 郑重承诺以下事项： 1、我保证所提交的信息(包括本人所提供的所有申请材料)真实准确，并保证与网上填报信息一致，信息修改、虚假或错误由本人自负； 2、自觉服从考试组织部门的统一安排，接受监考人员的检查、监督和管理； 3、保证在考试中诚实守信，自觉遵守国家有关研究生招生考试法规、考试纪律和考试规则，如有违法、违纪、违规行为，自觉服从监考人员根据国家有关规定所作出的处罚决定，接受处罚。 </div> <div> 考生（承诺人）签名： 年 月 日 考生承诺签字供现场审核 </div>

请根据招生单位要求在规定时间内提供其他相关材料

二.材料 2.身份证正反面复印后扫描件



复印在1页后扫描

三.材料3.本科和硕士学历、学位证书，应届生在读证明

371

302

70

普通高等学校

毕业证书

学生 性别 男，一九九六年十月二十一日生，于二〇一八年九月至二〇二〇年六月在本校专业 二 年制 本 科学习，修完教学计划规定的全部课程，成绩合格，准予毕业。

校 名

校 长：

证书编号

二〇二〇年 六 月 九 日

中华人民共和国教育部学历证书查询网址：<http://www.chsi.com.cn>



学士学位证书

，男， 年 月 日生。在

专业完成了本科学习计划，业已

毕业，经审核符合《中华人民共和国学位条例》的规定，授予 理学
学士学位。

校 长

学位评定委员会主席

证书编号：

二〇二〇年 六 月 九 日

(普通高等教育本科毕业生)

报考北京市结核病胸部肿瘤研究所博士研究生 在 读 证 明

兹证明_____, 身份证号_____,
男/女, _____年____月____日出生, 自____年____月起
在_____大学_____学院_____专业攻读硕士学位
研究生, 培养类型为_____学位(学术学位/专业学位),
学制_____年, 录取类别为_____ (定向/非定向), 拟
于_____年____月毕业。

不能空项目

(大学/学院) 研究生院 (部/处) (盖章)

年 月 日

四.材料 4.本科和硕士成绩单



本 科 生 成 绩 单

研究方向：

[illegible]

加*的为必修课

专业课加权平均分: 0.00

完 培美办公室

23-09-06

成绩单专用章

PEIJIANG UNION MEDICAL COLLEGE GRADUATE SCHOOL



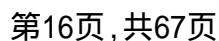
学号: TB20210420xx 姓名: xxxxxx 性别: 女 导师: xx
 年级: 2021 学制: 3 院系: 结核病胸部肿瘤所
 专业: 免疫学 研究方向:

加*的为必修课

必修课加权平均分: 84.44

专业课加权平均分: 0.00

2023-09-06



五.材料 5.思想政治情况表

首都医科大学

2025 年报考攻读博士学位研究生思想政治情况表

[illegible]

注：1.本表可复印使用，手工填写或电子输入均可。

2.本表签字盖章后交予录取学院教育处。

最迟面试前需提供原件供查验

电子版材料若不能提供，此页应为空白页，注明预计提供时间

六.材料 6.英语水平成绩单或证明

全国大学英语六级考试 成绩报告单



姓 名:
学 校:
院 系:
身份证号:

笔 试

准考证号:

考试时间:

口 试

准考证号: —

等级

—

考试时间: —

成绩报告单编号:



七.材料8.取得的科研成果

(1) Xu J, Zanvit P, Hu L, Tseng PY, Liu N, **Wang F**, Liu O, Zhang D, Jin W, Guo N, Han Y, Yin J, Cain A, Hoon MA, Wang S, Chen W. The Cytokine TGF- β Induces Interleukin-31 Expression from Dermal Dendritic Cells to Activate Sensory Neurons and Stimulate Wound Itching. *Immunity*. 2020 Aug 18;53(2):371-383.e5. doi: 10.1016/j.immuni.2020.06.023. Epub 2020 Jul 15. PMID: 32673566; PMCID: PMC7362873.

(2) JXu RC, **Wang F**, Sun JL, Abuduwaili W, Zhang GC, Liu ZY, Liu TT, Dong L, Shen XZ, Zhu JM. A novel murine model of combined hepatocellular carcinoma and intrahepatic cholangiocarcinoma. *J Transl Med*. 2022 Dec 9;20(1):579. doi: 10.1186/s12967-022-03791-z. PMID: 36494846; PMCID: PMC9733131.

Article

The Cytokine TGF- β Induces Interleukin-31 Expression from Dermal Dendritic Cells to Activate Sensory Neurons and Stimulate Wound Itching

Junji Xu,¹ Peter Zanvit,¹ Lei Hu,² Pang-Yen Tseng,³ Na Liu,¹ Fu Wang,^{1,4} Ousheng Liu,^{1,5} Dunfang Zhang,¹ Wenwen Jin,¹ Nancy Guo,¹ Yichen Han,¹ Jessica Yin,¹ Alexander Cain,¹ Mark A. Hoon,³ Songlin Wang,² and WanJun Chen^{1,6,*}

¹Mucosal Immunology Section, NIDCR, NIH, Bethesda, MD 20892, USA

²Molecular Laboratory for Gene Therapy & Tooth Regeneration, Beijing Key Laboratory of Tooth Regeneration and Function Reconstruction, School of Stomatology, Capital Medical University, Beijing 100050, China

³Molecular Genetics Section, Laboratory of Sensory Biology, NIDCR, NIH, Bethesda, MD 20892, USA

⁴Dalian Medical University, School of Stomatology, Dalian 114044, China

⁵Xiangya Stomatological Hospital & School of Stomatology, Central South University, Changsha 410000, China

⁶Lead Contact

*Correspondence: wchen@mail.nih.gov

<https://doi.org/10.1016/j.immuni.2020.06.023>

SUMMARY

Cutaneous wound healing is associated with the unpleasant sensation of itching. Here we investigated the mechanisms underlying this type of itch, focusing on the contribution of soluble factors released during healing. We found high amounts of interleukin 31 (IL-31) in skin wound tissue during the peak of itch responses. *IL31^{-/-}* mice lacked wound-induced itch responses. IL-31 was released by dermal conventional type 2 dendritic cells (cDC2s) recruited to wounds and increased itch sensory neuron sensitivity. Transfer of cDC2s isolated from late-stage wounds into healthy skin was sufficient to induce itching in a manner dependent on IL-31 expression. Addition of the cytokine TGF- β 1, which promotes wound healing, to dermal DCs *in vitro* was sufficient to induce *IL31* expression, and *Tgfb1^{fl/fl}* CD11c-Cre mice exhibited reduced scratching and decreased *IL31* expression in wounds *in vivo*. Thus, cDC2s promote itching during skin wound healing via a TGF- β -IL-31 axis with implications for treatment of wound itching.

INTRODUCTION

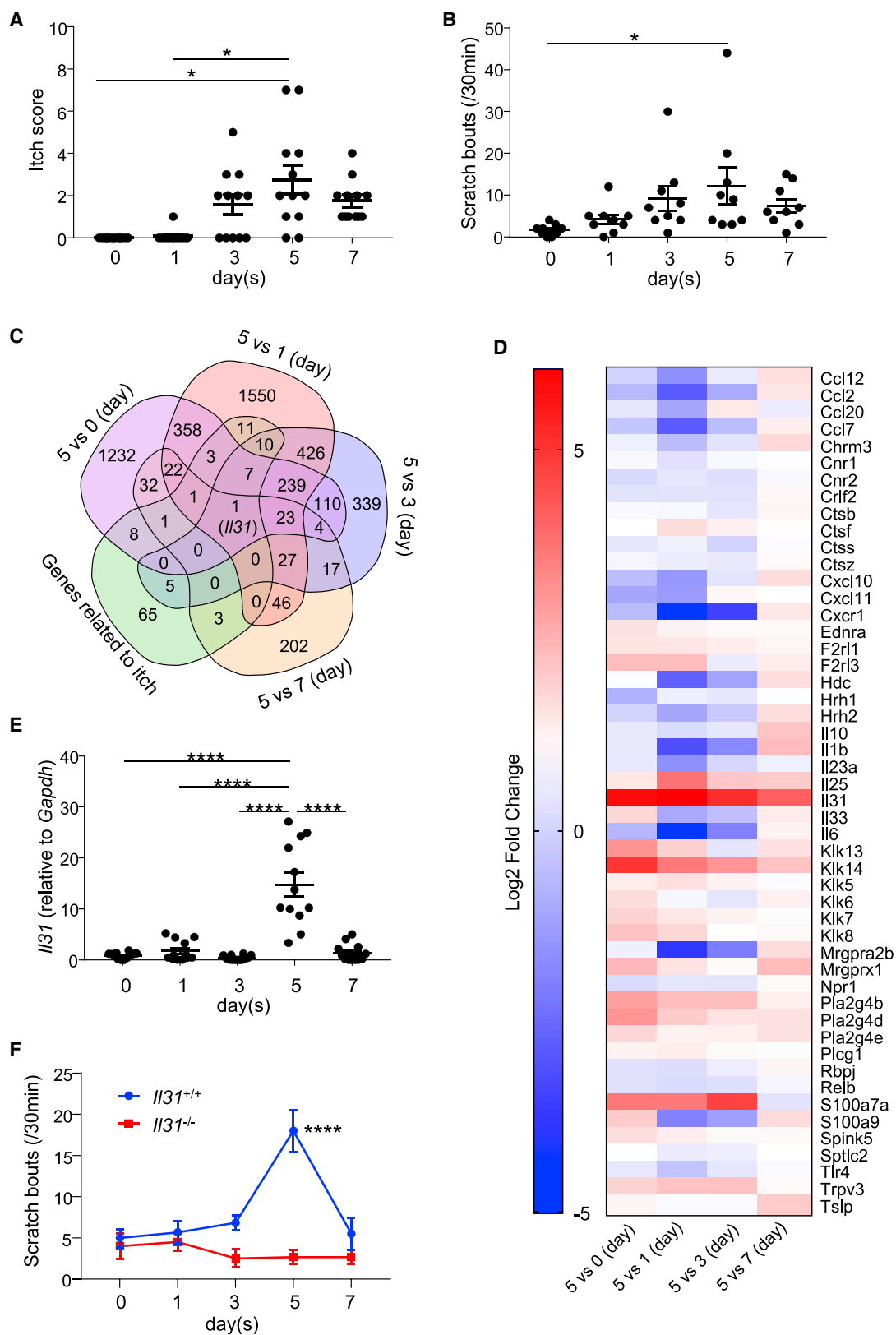
Cutaneous wound healing is a highly coordinated process that includes production of an ordered and dynamic inflammatory response involving multiple growth factors and cytokines (Ashcroft et al., 1999; Keyes et al., 2016; Massagué, 1999; Ross and Odland, 1968). For most wounds, itching is an unpleasant symptom that arises in the latter part of the healing process. Clinically, in patients with more extensive wounds (e.g., burns), there is more severe and persistent itching (Prasad et al., 2019; Parnell et al., 2012). Chemically induced itching is evoked by pruritogens activating primary afferent sensory neurons, which innervate the skin and have cell bodies in dorsal root ganglia (DRGs) and trigeminal ganglia. In mice, itch-inducing agents are detected by two nonoverlapping classes of sensory neurons that are thought, in part, to use the ion channel transient receptor potential cation channel subfamily V, member 1 (TRPV1) (Imamachi et al., 2009; Shim et al., 2007). One of these classes of neurons is marked by the transmitter natriuretic polypeptide B (NPPB) (Mishra and Hoon, 2013), which may convey pruritic signals to spinal cord circuits. The second class of neurons is defined by expression of Mas-related G-protein-coupled receptor a3 (Mrgpra3; Han et al., 2013), which express several

itch receptors, including Mrgpra3 and Mrgprc11. Activation of Nppb is sufficient to generate itch behavior (Huang et al., 2018) and is required for interleukin-31 (IL-31)-induced itching (Solinski et al., 2019b).

The interaction between the nervous system and the immune system has been suggested to be critically involved in normal homeostasis and pathogenic processes (Chavan et al., 2017). It has also become increasingly clear that neurological systems regulate immune responses through cell-cell contact (Tian et al., 2009) and/or release of soluble factors (Chavan et al., 2017). However, few studies have investigated the reverse direction; i.e., regulation of sensory neurons by the immune system. Specific inflammatory cytokines have been suggested to influence itching in skin (Bautista et al., 2014; Jin et al., 2009; Oetjen et al., 2017), suggesting that inflammation in the skin might play a role in development and pathogenesis of itching. However, the primary factor(s) and the underlying mechanisms of immune-mediated itching during wound healing remain elusive.

Here we utilized an experimental mouse model of wound healing to investigate the effects of immune responses on itching. We showed that IL-31, a prominent cytokine implicated previously in itching (Cevikbas et al., 2014; Dillon et al., 2004), was upregulated in skin wound tissue on the fifth day of healing, when itch





(legend on next page)

responses are maximal. We confirmed the itch-promoting effects of IL-31 on the skin and elucidated that IL-31 increased expression of the transduction channel TRPV1 and potentiated calcium influx in DRG neurons. Importantly, we also showed that the major cellular source of IL-31 production is dermal conventional type 2 dendritic cells (cDC2s).

RESULTS

Itch Responses and Changes in IL-31 Expression Follow Similar Time Courses during Wound Repair

To determine the progression of itch responses during skin wound healing, we monitored pruritus elicited by acute wound healing in humans and mice. For human subjects, we evaluated pruritus in 12 patients (diagnosed with a superficial cyst or benign tumor) using questionnaires for pruritus self-assessment prior to and every other day after surgery, employing a 10-cm visual analog scale (VAS; see [STAR Methods](#) for details). We observed that, in most patients, pruritus reached a peak on the fifth day after surgery ([Figure 1A](#)). Next we used an experimental mouse model of skin wound healing ([Ashcroft et al., 2000](#); [Figure S1](#)) and found that, similar to humans, mouse scratching responses ([Video S1](#)) were maximal on the fifth day of healing ([Figure 1B](#)).

To investigate whether there are soluble factor(s) present in wounded skin produced by immune cells during wound healing, which might be responsible for itching, we collected tissue and sequenced RNA transcripts several times before and during wound healing. For an unbiased analysis, we examined RNA sequencing (RNA-seq) reads, exploring changes in expression of all genes and focusing on those whose expression changes over the course of the healing process. We hypothesized that the expression of factors contributing to itching would peak at about the same time as itch responses. Next we examined genes, based on published literature ([Bautista et al., 2014](#); [Nattkemper et al., 2018](#); [Table S1](#)), that might be involved in this process. Using these criteria, we uncovered IL-31 as a candidate for induction of itching after cutaneous incision ([Figures 1C and 1D](#); [Table S2](#)). Confirming our RNA-seq analysis, real-time quantitative polymerase chain reaction (qPCR) and ELISA showed that there was increased expression of IL-31 throughout wound healing that peaked on day 5 after incision ([Figure 1E](#); [Figure S2A](#)).

IL-31 Is Responsible for Itch Responses during Wound Healing

If IL-31 is responsible for itch responses during wound healing, then we predicted that administration of additional IL-31 should further potentiate these responses. To test this, we injected IL-31 (30 ng/site, intradermally [i.d.]) into wounds starting on day 4 (see [STAR Methods](#) for details). In line with our hypothesis, mice treated with additional IL-31 displayed a higher number of scratching bouts compared with untreated animals ([Figure S2B](#)). To further investigate the role of IL-31 in itching during wound healing, we used *Il31*^{−/−} mice ([Figure S2C](#)). Corroborating a role of IL-31 in wound-induced itching, *Il31*^{−/−} mice scratched much less than wild-type mice on day 5 of wound healing ([Figure 1F](#)). A similar phenomenon was observed when bone marrow from *Il31*^{−/−} mice was transferred into irradiated C57BL/6 recipients ([Figures S2D and S2E](#)), indicating that hematopoietic cells, and possibly leukocytes, might be the main source of secreted IL-31.

IL-31 Increases Itch Sensory Neuron Sensitivity

Next, using RT-PCR, we compared the gene expression of molecules associated with signal transduction in DRGs that innervate the wound site between baseline and 5 days after incision. This comparison uncovered that expressions of *Il31ra*, *Trpv1*, and *Nppb* was upregulated during healing in sensory neurons, whereas expression of *Trpa1* did not change significantly ([Figures S3A–S3D](#)). Because DRG neurons are a heterogeneous population, *Trpv1*-lineage reporter mice (*Trpv1*-tdTomato mice) were also used to enrich for transcripts present in itch sensory neurons ([Mishra et al., 2011](#)). qPCR showed that *Il31ra*, *Trpv1*, and *Nppb* ([Figures 2A–2C](#)) were upregulated in sorted DRGs of *Trpv1*-lineage mice (which innervate wounds on day 5 after incision). This result is consistent with IL-31 being involved in induction of increased itch sensitivity in sensory neurons. To further test this hypothesis, we treated mouse DRG sensory neurons *in vitro* with IL-31. We found that IL-31 treatment on its own was sufficient to induce upregulation of *Trpv1*, *Il31ra*, and *Nppb* expression ([Figures S3E–S3G](#)). In addition, IL-31 treatment for 24 h could potentiate capsaicin (50 nM)-stimulated calcium influx in cultured DRG neurons ([Figures 2D, S3H, and S3I](#)) and could slightly increase the number of capsaicin-responding neurons in functional assays ([Figure S3J](#)). These results suggest that IL-31 may increase the expression of key signal transduction molecules in sensory neurons and that it can sensitize these nerves.

Figure 1. Pruritus Elicited by Acute Wound Healing and IL-31 Is Important for Itch during Wound Healing

(A) 12 patients with 1- to 3-cm sterile surgical wounds who experienced pruritus were surveyed over 7 days and asked to score the level of itching they felt on each day. One-way ANOVA was used for comparisons. Bars represent means ± SEM. **p* < 0.05.
(B) A mouse wound healing model was established by making 2 equidistant, 1 cm, full-thickness incisional wounds through the dorsal skin and left to heal. The number of scratching bouts per 30 min of observation were measured for 7 days following wounding. Data are from 3 independent experiments (*n* = 9) and were analyzed with a one-way ANOVA for comparisons. Bars represent means ± SEM. **p* < 0.05.
(C and D) Mouse wound skin at different time points was harvested, followed by RNA-seq of the mRNAs. The Venn diagram (C) shows overlapping of the genes that were significantly changed (*p* < 0.01) on the fifth day versus other time points of wound healing and genes related to itching based on published literature. The heatmap (D) shows all the itch-associated genes which changed on the fifth day were compared with any other time points. For RNA-seq, 2 wound tissues from one animal were pooled, and 3 animals were used per time point.
(E) The expression of IL-31 in wounds was confirmed by qPCR. Data are from 3 independent duplicated experiments (*n* = 12) and were analyzed with a one-way ANOVA for comparisons. Bars represent means ± SEM. *****p* < 0.0001.
(F) Itching behaviors of *Il31*^{−/−} mice during wound healing were compared with wild-type mice. Data are pooled from 2 independent experiments (*n* = 6) and represented as mean ± SEM; two-way ANOVA was used. *****p* < 0.0001.
See also [Figure S2](#) and [Tables S1 and S2](#) for more details.

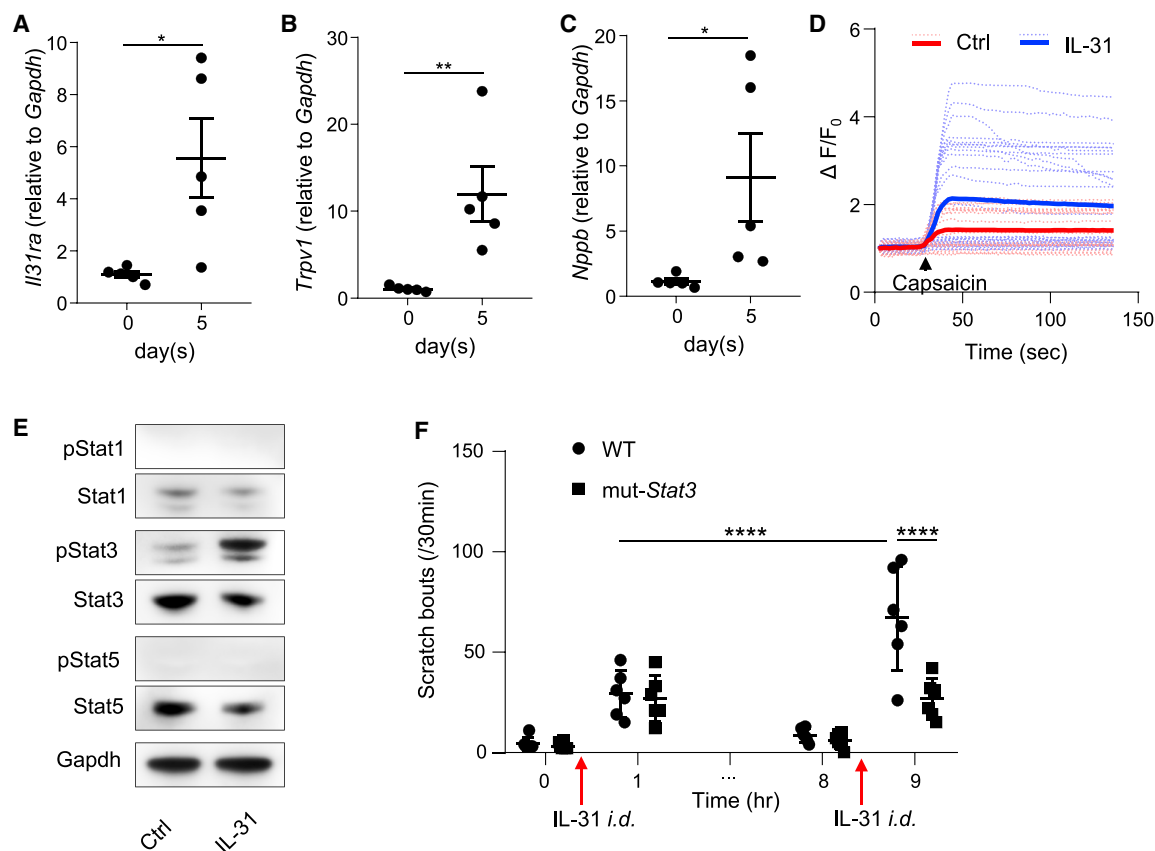


Figure 2. IL-31 Increases Itch Sensory Neuron Sensitivity

(A–C) TRPV1+ cells from DRGs that innervate the fifth day's wounds in *Trpv1*-lineage reporter mice (*Trpv1*-tdTomato mice) were sorted by flow cytometry, and the expression of *Il31ra* (A), *Trpv1* (B), and *Nppb* (C) in these TRPV1+ cells that innervate the fifth day's wounds were compared with TRPV1+ cells that innervate naive skin in normal controls by qPCR. Data were from 2 independent experiments (n = 5), and each sample was pooled from 2 mice. Student's t test was used for comparisons. Bars represent means \pm SEM. *p < 0.05, **p < 0.01.

(D) The calcium transient in capsaicin (50 nM) was observed in DRG neurons treated with IL-31 (10 ng/mL) for 24 h and in untreated neurons. The solid blue and red lines were representative images (mean values) and dash lines were individual traces.

(E) Phosphorylation of Stat3 was detected by western blot in DRG neurons treated with IL-31 (10 ng/mL) for 24 h. Data are representative of 3 independent experiments.

(F) Scratching bouts of mut-Stat3 mice were counted after the first IL-31 injection (1 μ g/site, i.d.) and compared with wild-type mice. 8 h after the first IL-31 injection, the second IL-31 injection was administered, and the itching behaviors were again observed. Data were from 2 independent experiments (n = 6) and analyzed with a two-way ANOVA for comparisons. Bars represent means \pm SEM. ****p < 0.0001.

See also Figure S3 for more details.

Because IL-31, via the IL-31ra receptor, may induce changes in gene expression and neural activity through a Jak1-mediated pathway (Zhang et al., 2008), we investigated potential additional downstream effectors of IL-31 activation. To do this, we explored, in DRG neurons, which Stat molecules might be regulated by IL-31 treatment. These experiments revealed that IL-31 induces phosphorylation of Stat3 (Figure 2E). If Stat3 phosphorylation is required for potentiation of neuronal activity, then administration of a specific Stat3 inhibitor should attenuate IL-31-induced increases in calcium responses to capsaicin. Indeed, the Stat3 inhibitor S31-201 blocked IL-31-stimulated increases in calcium influx and the numbers of neurons responding to capsaicin (Figures S3K–S3M). Furthermore, S31-201 inhibited IL-31-induced upregulation of *Trpv1* and *Il31ra* expression (Figures S3N and S3O), indicating that these IL-31-mediated effects are Stat3 dependent.

We wondered how IL-31 acts on itch sensory neurons to alter gene expression. To investigate this, we tested the effects of IL-31 on neurons at different time points. We uncovered that Stat3 phosphorylation occurred within 15 min after IL-31 treatment (Figure S3P), but the increase in *Il31ra* and *Trpv1* expression was delayed and started between 1 and 3 h later (Figures S3Q and S3R). Furthermore, when we injected IL-31 (1 μ g/site i.d.) into mutant (mut)-Stat3 mice, the same amount of initial scratching was observed in mut-Stat3 mice as in wild-type control mice. However, 8 h after the first IL-31 injection, when we gave a second IL-31 dose, scratching was increased markedly in wild-type mice but not in mut-Stat3 animals (Figure 2F). In addition, concordant with results from our experiments with a Stat3 inhibitor, *Il31ra* and *Trpv1* gene expression in DRGs that innervate the injected area of skin also showed that IL-31 injection *in vivo* could not upregulate these two genes in the short

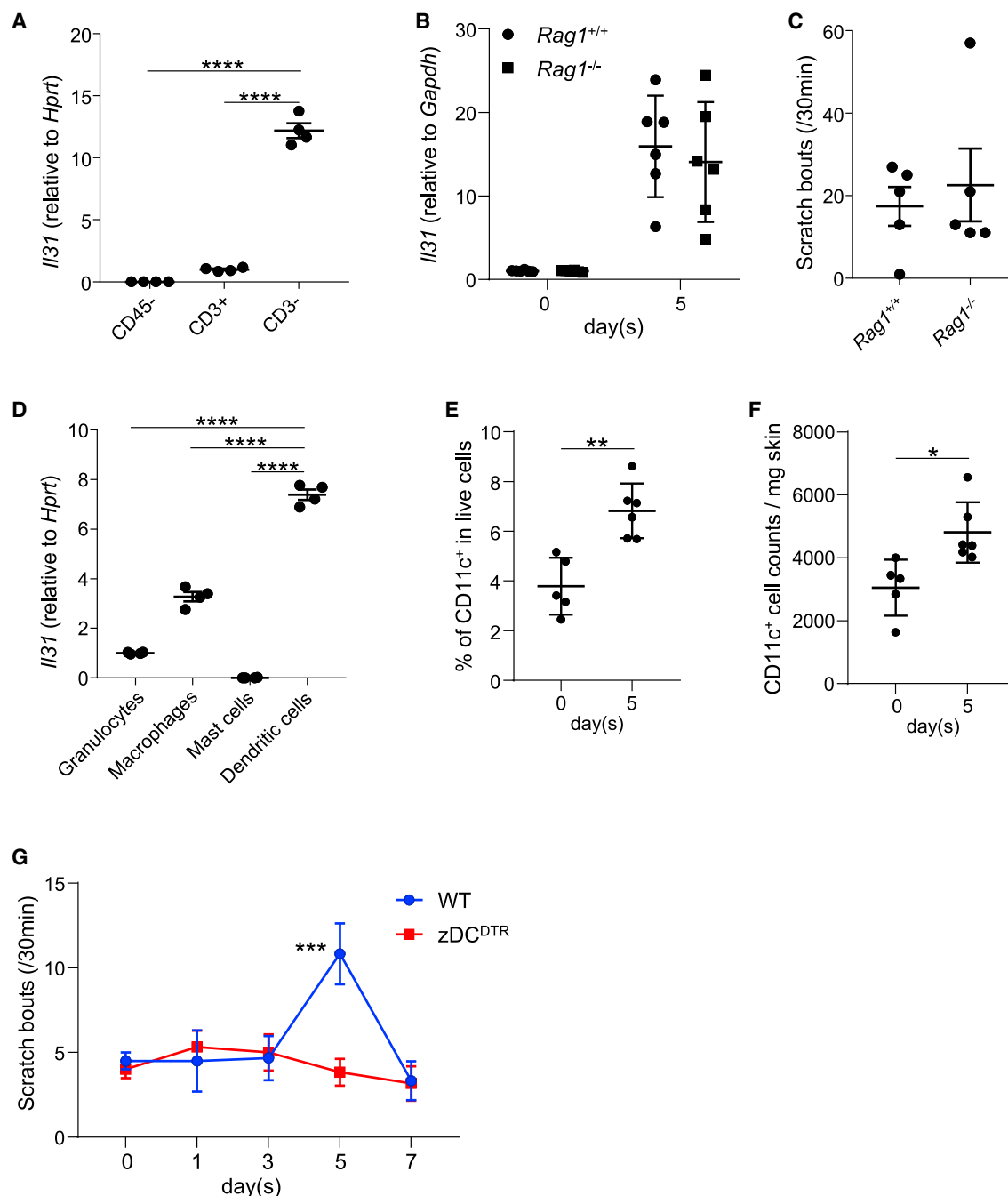


Figure 3. Dermal DCs Are a Key Source of IL-31 in Wounds

(A) *Il31* gene expression was determined in CD45⁻ cells, CD45⁺CD3⁺ cells, and CD45⁺CD3⁻ cells sorted from fifth-day wounds tissue by qPCR. Data were from 2 independent experiments with 2 samples each time, and each sample was pooled from 4 wounds in 2 mice. Data were analyzed with one-way ANOVA for comparisons. Bars represent means \pm SEM. **** p < 0.0001.

(B) Expression of IL-31 in wounds on the fifth day were tested in *Rag1*^{-/-} mice and wild-type mice by real-time PCR. Data are from 3 independent experiments (n = 6), and two-way ANOVA was used for comparison. Bars represent means \pm SEM.

(C) Scratching behaviors were observed in *Rag1*^{-/-} mice before and on the fifth day of wound healing. Data are from 2 independent experiments (n = 5); Student's t test was used. Bars represent means \pm SEM.

(D) DCs (CD45⁺CD3⁻CD11c⁺MHC II⁺), macrophages (CD45⁺CD3⁻CD11c⁺CD11b⁺F4/80⁺), granulocytes (CD45⁺CD3⁻CD11c⁻CD11b⁺F4/80⁺), and mast cells (CD45⁺CD3⁻CD11c⁻CD11b⁺FceR1a⁺) were sorted from fifth-day wounds, and the expression of *Il31* was determined by real-time PCR. Data were from 2 independent experiments with 2 samples each time, and each sample was pooled from 4 wounds in 2 mice. Data were analyzed with one-way ANOVA for comparisons. Bars represent means \pm SEM. **** p < 0.0001.

(legend continued on next page)

term (within 1 h) but could increase expression over the long term (8 h) in wild-type mice (Figures S3S and S3T). Notably, this IL-31-induced upregulation did not occur in *mut-Stat3* mice (Figures S3S and S3T). Furthermore, to investigate whether scratching during wound healing is associated with Nppb/Npr1, we injected an Nppb receptor agonist, Npr1 (JS-11, 5 mg/kg intraperitoneally [i.p.]) into mice on day 5 of wound healing (Solinski et al., 2019a). JS-11-treated mice exhibited attenuated scratching 15 min after injection (Figure S3U), indicating that the wound-associated itch is Nppb/Npr1 dependent. Taken together, our results suggest that IL-31 has short-term effects that are Stat3 independent and has longer-term effects on neuronal sensitivity, as evidenced by Stat3-dependent increased *Il31ra* and *Trpv1* expression.

Dendritic Cells Cause Itching during Wound Healing

We next investigated the source of IL-31 in the skin during wound healing. IL-31 has been classified as a T helper 2 (Th2) cytokine (Dillon et al., 2004); however, CD3⁺ T cells sorted from wound tissues on day 5 after incision expressed much lower *Il31* than CD3⁺ non-T cells within the CD45⁺ immune cell population (Figure 3A). Our analysis also revealed that CD45⁺ non-immune cells expressed minimal *Il31* mRNA (Figure 3A). Confirming these results, the expression of IL-31 detected in wounds from *Rag1*^{−/−} mice was the same as in control mice (Figures 3B and S4A), indicating that T cells or B cells are not a major source of IL-31 in wounds. Again, in line with B and T cells having minimal involvement in wound itching, *Rag1*^{−/−} mice exhibited similar wound-induced scratch behaviors as wild-type mice (Figure 3C). When we further fractionated CD3⁺ non-T cells from wound skin, we found that dendritic cells (DCs) had higher expression of *Il31* compared with macrophages, granulocytes, and mast cells (Figure 3D). Moreover, higher numbers of CD11c⁺ cells were found in day 5 wounds compared with normal skin (Figures 3E, 3F, and S4B).

If DCs are the major source of IL-31 in wounds, then depletion of DCs in the skin should alleviate itching during wound healing. To test this, we made a previously characterized cDC depletion mouse model (Meredith et al., 2012) by transferring bone marrow from zDC^{DTR} mice, in which human diphtheria toxin receptor is expressed in cDCs, but not monocytes or other immune cell populations, into irradiated C57BL/6 hosts and injecting diphtheria toxin (DT) to specifically deplete cDCs (Figure S4C). These mice did not exhibit increased itch behavior during wound healing (Figure 3G), indicating that cDCs may be the main source of IL-31. Furthermore, *Il31* expression in the wounds of these mice was also lower than in control animals (Figure S4E), but these mice displayed no change in wound closure and healing (Figure S4D). These results establish that DCs are the primary source of IL-31, which causes itching during wound healing.

cDC2s Are a Key Source of IL-31 in Wounds

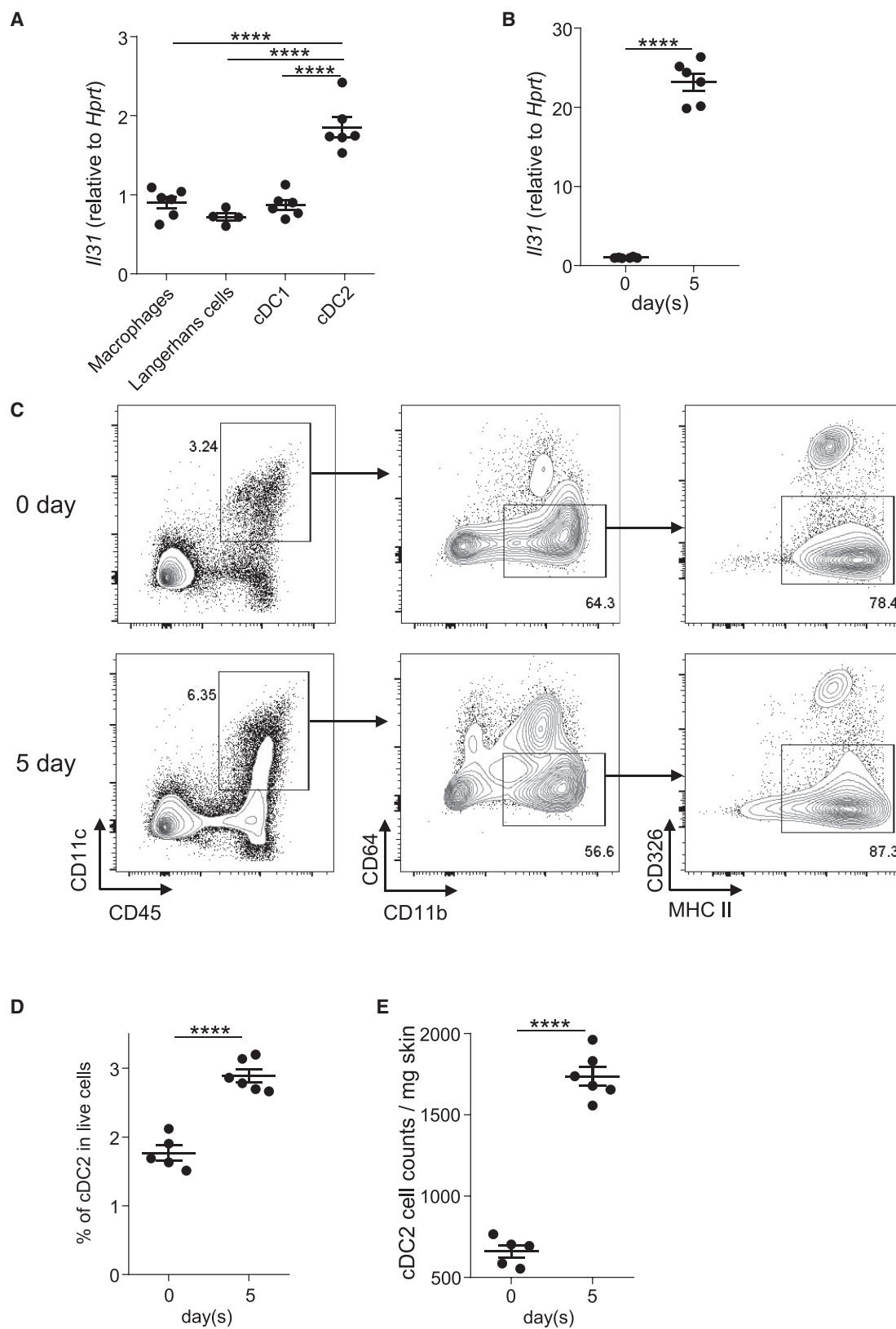
To determine which subset of DCs express IL-31, we next sorted Langerhans cells (LCs), type 1 cDCs (cDC1s), cDC2s, as well as macrophages and found that cDC2s expressed the highest level of *Il31* of all of these types of cells (Figure 4A). We further used *Lang*^{DTR} mice, which express the human DT receptor (DTR) downstream of the internal stop codon of the *Langerin* gene, to deplete LCs (Figures S5A–S5C). We also used a well-characterized monocyte/macrophage depletion mouse model by crossing *Lys2*^{Cre} mice and *Csf1r*^{DTR} mice (Schreiber et al., 2013) (hereafter called MM^{DTR} mice). In *Csf1r*^{DTR} mice, a DTR preceded by a loxP-flanked transcriptional stop element under control of the *Csf1r* promoter, expression of Cre recombinase excises the stop element and allows transcription and translation of DTR in cells expressing *Csf1r*, so administering DT to MM^{DTR} mice could deplete macrophages in the skin (Figures S5D–S5F). Itch behaviors during wound healing in these two models were observed. Both models have normal frequencies of cDCs in the skin (Figures S5A and S5D) and normal itch behavior on day 5 during wound healing. We also compared *Il31* expression between dermal cDC1s and cDC2s by using CD103 and CD207 as markers to distinguish dermal cDC1s and cDC2s (Kashem et al., 2017) and found that dermal cDC2s indeed expressed higher levels of *Il31* than cDC1 (Figures S5G and S5H). Moreover, *Il31* mRNA expression in cDC2s from day 5 wounds was much higher than in cDC2s from normal skin (Figure 4B). The proportions (Figures 4C and 4D) and total numbers of cDC2s (Figure 4E) were also increased on day 5 after incision compared with naive skin.

These results suggest that cDC2s are the likely source of *Il31*, producing increased scratching during wound healing. To further validate this, we examined whether cDC2s are sufficient to elicit wound-like itching. We purified cDC2s from day 5 wounds or normal skin and injected them intradermally in uninjured recipient mice (1.5 × 10⁴ cells per site). cDC2s from wound sites increased scratching in recipient mice 3 h after injection (Video S2) but cDC2s from normal skin did not (Figure 5A). In addition, consistent with these cDC2s evoking itching through activation of an IL-31 process, expression of *Il31ra* (Figure 5B), *Trpv1* (Figure 5C), and *Nppb* (Figure 5D) was upregulated in DRGs of recipient mice that innervated the skin around cDC2 injection. To probe whether scratching evoked by dermal cDC2 administration elicits itching or nociceptive sensations, we turned to the cheek model (Shimada and LaMotte, 2008). In this model, scratch responses to intradermal injection of a substance into the face are interpreted to be caused by itching, whereas wipe responses are believed to be triggered by nociception (production of pain). Consistent with cDCs provoking itching, injection of cDC2s from day 5 of wound healing into the cheek caused prominent scratching compared with cDCs from naive mice (Figure 5E). In contrast, wiping responses were similar for cDCs from

(E and F) The frequency (E) and numbers (F) of CD11c⁺ cells from day 5 wounds was calculated and compared with those from normal skin. Data were from 3 independent experiments (n = 5–6), analyzed with Student's t test for comparisons. Bars represent means ± SEM. ****p < 0.0001.

(G) Itching behaviors during wound healing were observed in diphtheria toxin (DT)-treated (i.p., 500 ng/mouse for the first time and 100 ng/mouse on all subsequent days) zDC^{DTR}-to-C57BL/6 bone marrow chimera mice and were compared with DT-treated C57BL/6-to-C57BL/6 bone marrow chimera mice (WT [wild-type]). Data were pooled from 6 mice for each condition in two independent experiments and are represented as mean ± SEM. Two-way ANOVA was used for multiple comparisons. ***p < 0.001.

See also Figure S4 for more details.



(legend on next page)

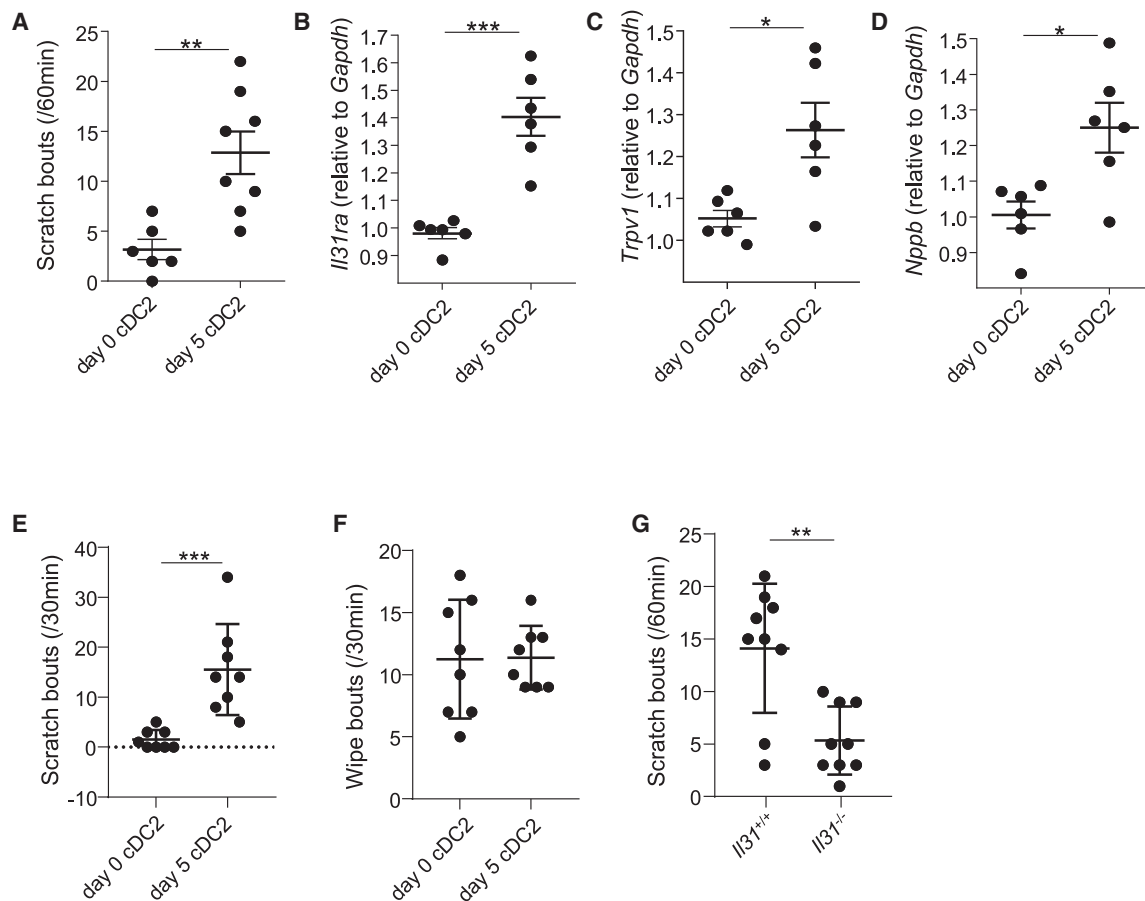


Figure 5. Administration of Late Wound Stage Dermal cDC2s Evokes Itch Responses

(A–D) Dermal cDC2s sorted from fifth-day wounds or normal skin was injected intradermally to the dorsal area of normal B6 mice at 15,000 per site, and the scratching behaviors were counted 3 h after injection (A). The expression of *Il31ra* (B), *Trpv1* (C), and *Nppb* (D) in DRGs that innervate the back skin around the dermal cDC2-injected area was also determined by real-time PCR. Data were from 2 independent experiments with 3–4 mice each time. Student's t test was used for comparison. Bars represent means \pm SEM. * $p < 0.05$, ** $p < 0.01$, *** $p < 0.001$.

(E and F) The numbers of scratching behaviors (E) and wiping behaviors (F) were counted after injection of cDC2s from fifth-day wounds or normal skin to cheeks of mice. Each circle represents one mouse. Data are from 2 independent experiments ($n = 8$), and Student's t test was used. Bars represent means \pm SEM. *** $p < 0.001$.

(G) Scratching bouts were counted in recipient mice that were injected with cDC2s from fifth-day wounds of *Il31*^{-/-} mice or WT mice. Data were pooled from 3 independent experiments ($n = 9$). Each circle represents one mouse. Student's t test was used. Bars represent means \pm SEM. ** $p < 0.01$.

See also Figure S5 for more information.

naive and day 5 wounds (Figure 5F). Supporting this conclusion itch responses evoked by day 5 wound cDC2s from *Il31*^{-/-} mice were similar to the behavior elicited by administration of cDCs from naive skin (Figure 5G). Taken together, these results suggest that cDC2 is the major source of IL-31 in wounds, which produces itching associated with wound repair.

TGF- β Increases IL-31 in Dermal cDC2s

Because cDC2s in healthy skin contain low amounts of IL-31, we wondered which cues in wounds might be involved in increasing its expression. The cytokines IL-1 β , IL-6, IL-17a, transforming growth factor β 1 (TGF- β 1), and tumor necrosis factor alpha (TNF- α) have been reported to be important participants in

Figure 4. IL-31 in Wounds Was Mostly from Dermal cDC2s

(A) Macrophages (CD45⁺CD3⁻CD11c⁻CD64⁺CD11b⁺F4/80⁺), LCs (CD45⁺CD3⁻CD11c⁺CD326⁺), dermal cDC2s (CD45⁺CD3⁻CD11c⁺CD326⁻CD64⁻CD11b⁺MHC II⁺), and dermal cDC1s (CD3⁻CD11c⁺CD326⁻CD64⁻CD11b⁻MHC II⁺) were sorted from fifth-day wounds, and *Il31* expression was determined by real-time PCR. Data were from 2–3 independent experiments with 2 samples each time, and each sample was pooled from 4 wounds in 2 mice. Data were analyzed with one-way ANOVA for comparisons. Bars represent means \pm SEM. **** $p < 0.0001$.

(B) *Il31* gene expression in dermal cDC2 from fifth-day wounds was compared with cDC2s from normal skin by real-time PCR. Data are from 3 independent experiments with 2 samples each time, and each sample was pooled from 4 wounds in 2 mice. Data were analyzed with Student's t test for comparisons. Bars represent means \pm SEM. **** $p < 0.0001$.

(C–E) Flow cytometer analysis showed that the frequency (C and D) and total numbers of dermal cDC2s (CD45⁺CD11c⁺CD64⁻CD11b⁺MHC II⁺CD326⁻) (E) were increased in fifth-day wound skin tissues compared with normal skin. In (D) and (E), each circle represents one mouse. Data were from 3 independent experiments ($n = 5–6$), and Student's t test was used. Bars represent means \pm SEM. **** $p < 0.0001$.

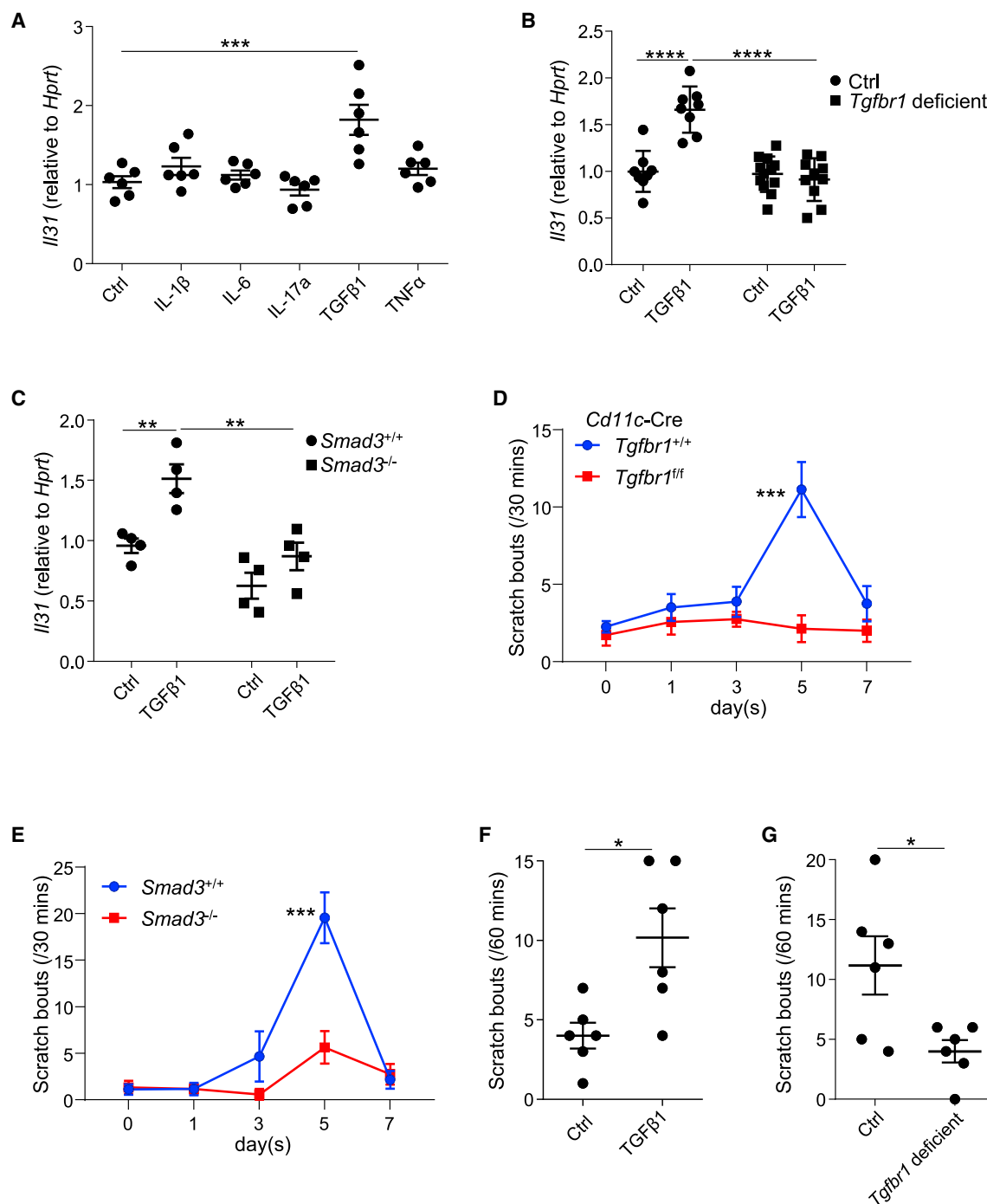


Figure 6. TGF- β Increases IL-31 in Dermal cDC2

(A) IL-1 β (10 ng/mL), IL-6 (50 ng/mL), IL-17a (10 ng/mL), TGF- β 1 (2 ng/mL), and TNF- α (10 ng/mL) were used *in vitro* to treat cDC2s sorted from healthy skin individually, and IL-31 expression in dermal cDC2s was determined 6 h after treatment. Data were from 3 independent experiments (n = 6), and each circle represents one culture well. Data were analyzed with one-way ANOVA for comparisons. Bars represent means \pm SEM. ***p < 0.001.

(B and C) The expression of IL-31 in TGF- β 1-treated dermal cDC2s from *Tgfr1*-deficient mice (tamoxifen-treated *Tgfr1*^{fl/fl} *Ert2*-Cre mice) (B) and *Smad3*^{-/-} mice (C) were determined and compared with WT dermal cDC2s. Data were from 2 independent experiments (n = 4–8). Each circle represents one culture well, and two-way ANOVA was used for comparisons. Bars represent means \pm SEM. ****p < 0.0001.

(D and E) The wound healing model was set up in *Tgfr1*^{fl/fl} *Cd11c*-Cre (D) and *Smad3*^{-/-} mice (E). Itching behaviors were observed in *Tgfr1*^{fl/fl} *Cd11c*-Cre mice and *Smad3*^{-/-} mice and compared with WT controls. Data were from 3 independent experiments (n = 6–8) and represented as mean \pm SEM. Two-way ANOVA was used for comparisons. ***p < 0.001.

(legend continued on next page)

coordinating wound repair (Barrientos et al., 2008; Mast and Schultz, 1996). Therefore, we tested the effects of these cytokines on induction of IL-31 expression in isolated dermal cDC2s *in vitro*. Unexpectedly, only TGF- β 1 substantially increased *Il31* expression in cDC2s from normal skin (Figure 6A). Consistent with TGF- β 1 inducing IL-31 in dermal cDC2s, we found that TGF- β 1 expression was raised between days 3 and 5 after incision (Figure S6A). Because Smad3 is downstream of canonical TGF- β signaling, we used a TGF- β receptor I (TGF- β RI) inhibitor (SB431542) or a selective Smad3 inhibitor (SIS3) under TGF- β 1 culture conditions. Corroborating TGF- β RI and Smad3 as being part of the signal cascade for induction of *Il31* expression, their inhibitors reduced induction of IL-31 transcription (Figure S6B). Further substantiating the contribution of TGF- β 1 in induction of IL-31 expression, the increase in *Il31* expression in response to TGF- β is absent in dermal cDC2s from TGF- β RI global knockout mice (*Tgfbri*^{fl/fl} *Ert2*-Cre) (Figure 6B) and *Smad3*^{-/-} mice (Figure 6C), and *in vitro* TGF- β 1 treatment failed to increase *Il31* expression in dermal cDC2s from these knockout mice (Figures 6B and 6C). To further investigate the role of TGF- β RI in DCs during wound healing, we crossed *Cd11c*-Cre⁺ mice with *Tgfbri*^{fl/fl} mice to conditionally deplete TGF- β RI in DCs, whereas other types of cells were untouched. Histological staining showed that conditional depletion of TGF- β RI in DCs did not alter the speed of the wound healing process (Figure S6C). Like the *Tgfbri*^{fl/fl} *Ert2*-Cre mice, TGF- β 1 treatment also failed to increase *Il31* expression in dermal cDC2s from *Tgfbri*^{fl/fl} *CD11c*-Cre mice *in vitro* (Figure S6D). Compared with wild-type mice, *Tgfbri*^{fl/fl} *CD11c*-Cre mice exhibited reduced scratching behaviors (Figure 6D) and a lower *Il31* expression in wounds (Figure S6E) on day 5 after injury. Notably, expression of *Il31ra* (Figure S6F), *Trpv1* (Figure S6G), and *Nppb* (Figure S6H) were also not upregulated in the DRGs that innervated wounds. Furthermore, we generated *Tgfbri*^{fl/fl} *Lyz2*-Cre mice, in which TGF- β RI is eliminated on macrophages but not on DCs. These mice displayed a similar healing process and itching behaviors as wild-type mice (Figures S6J and S6K). Moreover, although the wound healing processes were accelerated (Figure S6L), scratch- and itch-related gene expression in *Smad3*^{-/-} mice also declined relative to control littermates at all time points (Figures 6E and S6M–S6O). Finally, intradermal administration, in recipient animals, of TGF- β 1-pretreated dermal cDC2s increased itch behavior (1.5×10^4 cells per site; Figure 6F). In contrast, TGF- β 1-treated dermal cDC2s isolated from *Tgfbri*^{fl/fl} *Ert2*-Cre mice (Figure 6G) and *Tgfbri*^{fl/fl} *CD11c*-Cre mice (Figure S6I) failed to elicit itch responses. Moreover, even at a low dose of injection (5,000 cells per site), TGF- β 1-treated dermal cDC2s could elicit itch responses (Figure S6P) and upregulate *Il31ra* gene expression in DRGs of recipient mice that innervated the skin injected with these cells, although no significant difference in *Trpv1* gene expression could be found (Figure S6Q),

whereas TGF- β 1-treated dermal cDC2s from *Tgfbri*^{fl/fl} *Ert2*-Cre mice failed to do so (Figures S6R and S6S). Together, these results demonstrate the crucial role of TGF- β signaling in IL-31 production in dermal cDC2s during wound healing.

DISCUSSION

In this study, we investigated the cellular and molecular mechanisms underlying itching during cutaneous wound healing, showing that TGF- β induces expression of IL-31 in dermal cDC2s and that this contributes to generation of scratch behavior through activation of sensory neurons. First we found a close association of the peak of itch responses and cutaneous IL-31 expression. Second, we showed that IL-31 has short-term effects evoking itching, which is Stat3 independent, and long-term effects on increasing the sensitivity of sensory neurons. Third, we established that dermal cDC2s are critical cellular sources of IL-31 during wound repair and that day 5 dermal cDC2s are sufficient to evoke itch responses in naive mice. Finally we demonstrate that IL-31 expression in cDC2s requires Smad-dependent TGF- β signaling. These findings provide the immunological and neurological underpinnings of the widely known sensation of itching that is experienced in the later stages of skin wound healing.

It is thought that many pruritogens evoke itching (Steinhoff et al., 2018; Trier and Kim, 2018), but the principle underlying the agents responsible for the itching induced during cutaneous repair have not been studied. Here we discovered that the cytokine IL-31, based on our unbiased RNA-seq analysis, qPCR, and protein analysis, was prominently expressed, peaking at approximately the same time when itching was most intense. In mice and humans, type 2 cytokine signaling contributes to itching (Oetjen et al., 2017), and IL-31 was initially described as a Th2 cytokine mainly related to dermatitis and some respiratory diseases (Bilsborough et al., 2010; Cevikbas et al., 2014; Dillon et al., 2004). Supporting this function of IL-31 in itching, anti-IL-31 receptor antibodies have been reported to relieve dermatitis in a mouse model and human patients (Kasutani et al., 2014; Ruzicka et al., 2017). Therefore, we propose that IL-31 is also a likely agent contributing to pruritus when the skin is recovering from injury, and a slow build-up of IL-31 causes the increasing prurceptive sensation that builds during wound healing during this process. For this reason, IL-31 might be a good target for treatment of pruritis in more extensive body surface areas, such as with burns.

We wondered why IL-31 might be elevated during wound healing and considered that it might influence immune cell functions at the repair site and, therefore, be important in wound closure or other processes producing an intact barrier. This idea was not borne out because, in *Il31*^{-/-} mice, we did not find significant changes in wound healing. This still does not answer what

(F) Dermal cDC2 from normal skin treated with or without TGF- β 1 for 24 h were injected (i.d., 15,000 cells per site) to the dorsal area of normal B6 mice, and scratching bouts on the dorsal area of dermal cDC2 recipients were counted 3 h after injection. Data were from 3 independent experiments, each circle represents one mouse (n = 6). Student's t test was used for comparison. Bars represent means \pm SEM. *p < 0.05.

(G) Dermal cDC2 from normal or *Tgfbri*-deficient mice (tamoxifen-treated *Tgfbri*^{fl/fl} *Ert2*-Cre mice) were also treated with TGF- β 1 for 24 h and injected into the dorsal area of normal B6 mice, and scratch counts were determined in recipients of dermal cDC2s. Data were from 3 independent experiments. Each circle represents one mouse (n = 6). Student's t test was used for comparison. Bars represent means \pm SEM. *p < 0.05.

See also Figure S6 for more details.

IL-31 might be doing, but it means that therapeutic agents neutralizing IL-31 would not impair wound recovery. Future experiments might investigate the reasons for elevated IL-31 during wound repair. In addition, studies have shown that IL-31 has roles in nerve growth (Feld et al., 2016) and neuropeptide release (Meng et al., 2018); it is reasonable that wound itching occurs when nerve fibers are remodeling into the dermis/epidermis.

IL-31 has been reported previously to acutely induce itching via activation of IL-31Ra on TRPV1⁺ sensory neurons, which innervate the skin (Cevikbas et al., 2014), and to also evoke delayed itching (Arai et al., 2013; Hawro et al., 2014). Here we showed that, at least in part, IL-31 may increase sensory neuron activity by upregulation of expression of molecules involved in signaling reception (*Il31Ra*), signal transduction (*Trpv1*), and signal transmission (*Nppb*). These increases in expression are long-term effects and are Stat3 dependent. In turn, this suggests that Stat3 might be another potential therapeutic target for use in IL-31-dependent itching.

In the dermis, cDCs are conventional resident DCs and have critical roles in guarding the host against invading pathogens while limiting tissue damage. They are involved in some pathologies, including infectious and parasitic diseases transmitted through the skin (Clausen and Stoitzner, 2015; Valladeau and Saeland, 2005). cDCs are the most abundant type of DCs in the healthy mouse dermis (Malissen et al., 2014; Tamoutounour et al., 2013); upon migration to draining lymph nodes, they can trigger Th2 cell differentiation (Kitajima and Ziegler, 2013) and induce production of regulatory T cells (Guilliams et al., 2010). For these reasons, their numbers are substantially increased at sites of barrier disruption. It has been reported previously that nociceptive sensory neurons, by interacting with dermal cDCs, can regulate the IL-23/IL-17 pathway and control cutaneous immune responses in a model of psoriasis (Riol-Blanco et al., 2014). Here we focused on the reverse direction and investigated how immune cells affect the peripheral nervous system and behavior. Our results show that elevated amounts of IL-31 in wounds is predominantly generated by dermal cDC2s. Therefore, our results show that there is reciprocal signaling between cutaneous cDC2s and peripheral sensory neurons, highlighting the importance of the interaction between the immune and nervous systems in the skin.

TGF- β signaling is crucial during wound healing; it has a broad spectrum effects on almost every cell type, including keratinocytes, fibroblasts, DCs, and monocytes (Ashcroft et al., 1999). TGF- β 1 is important for wound closure by facilitating fibroblast contraction in the collagen matrix (Meckmongkol et al., 2007) and development of hypertrophic and keloid scars (Colwell et al., 2005) and for inducing and sustaining activation of keloid fibroblasts (Wang et al., 2007). TGF- β 1 directs differentiation of monocytes into LCs and is crucial for the cutaneous contingent of migratory DCs (Felker et al., 2010). Moreover, TGF- β may induce tolerogenic DCs, which can skew effector T cell immune response into cells of a predominantly anti-inflammatory Th2-like phenotype or may induce generation of regulatory T cells (Chen et al., 2003; Esebanmen and Langridge, 2017; van Duiven-voorde et al., 2006). In this study, we expand the list of TGF- β functions to wound healing-induced itching by demonstrating that TGF- β signaling increases IL-31 production in dermal cDC2s.

Here we provide evidence of an IL-31-mediated effect on the sensory nervous system and mammalian behavior. By identifying this neuro-immunologic pathway and determining key mechanistic steps involved in this process, we identify potential therapeutic targets for itching that occurs during wound healing and potentially other conditions that disrupt the skin barrier and cause itching.

Limitations of Study

Although our study shows that IL-31 is responsible for itch responses during wound healing, it remains an exciting question whether there is any other biological function of IL-31 in that period. Future experiments might also investigate the reasons for elevated IL-31 during wound repair; it would be insightful to focus on the roles of IL-31 in nerve growth and neuropeptide release. Our study could be improved by some direct visual evidence of IL-31 expression in the skin, which we were unable to provide because of the coronavirus disease 2019 (COVID-19) pandemic.

STAR★METHODS

Detailed methods are provided in the online version of this paper and include the following:

- KEY RESOURCES TABLE
- RESOURCE AVAILABILITY
 - Lead Contact
 - Materials Availability
 - Data and Code Availability
- EXPERIMENTAL MODELS AND SUBJECT DETAILS
 - Human data of pruritus questionnaires
 - Mice
- METHOD DETAILS
 - Enroll and exclusion criteria for human pruritus questionnaires
 - Bone marrow chimeras and diphtheria toxin injection
 - Murine wound healing
 - IL-31 intradermal injection
 - Pruriceptive behavior measurement
 - RNA-seq analysis
 - Cell culture of dorsal root ganglion neurons
 - Calcium image
 - Flow cytometry
 - Dermal conventional type 2 dendritic cells culture and injection
 - Real-time PCR
 - Antibodies and reagents
 - Statistical analysis

SUPPLEMENTAL INFORMATION

Supplemental Information can be found online at <https://doi.org/10.1016/j.immuni.2020.06.023>.

ACKNOWLEDGMENTS

This research was supported by the Intramural Research Program of the U.S. National Institutes of Health (NIH), National Institute of Dental and Craniofacial Research (NIDCR). We thank Dr. Susumu Nakae (The Institute of Medical

Science, The University of Tokyo) for providing gene-mutated mice. We thank the NIDCR combined technical research core (ZIC DE000729-09) and imaging core for technical assistance.

AUTHOR CONTRIBUTIONS

J.X. designed and performed experiments, analyzed data, and wrote the manuscript. P.Z., L.H., D.Z., N.L., W.J., and Y.H. designed and performed experiments. P.-Y.T. provided critical methods and analyzed RNA sequence data. F.W., O.L., N.G., J.Y., A.C., and S.W. provided critical scientific input. M.A.H. supervised the study and wrote the manuscript. W.C. conceived, initiated, and supervised the whole study; designed experiments; and wrote the manuscript.

DECLARATION OF INTERESTS

The authors declare no competing interests.

Received: March 12, 2020

Revised: April 17, 2020

Accepted: June 22, 2020

Published: July 15, 2020

REFERENCES

- Arai, I., Tsuji, M., Takeda, H., Akiyama, N., and Saito, S. (2013). A single dose of interleukin-31 (IL-31) causes continuous itch-associated scratching behaviour in mice. *Exp. Dermatol.* 22, 669–671.
- Ashcroft, G.S., Yang, X., Glick, A.B., Weinstein, M., Letterio, J.L., Mizel, D.E., Anzano, M., Greenwell-Wild, T., Wahl, S.M., Deng, C., and Roberts, A.B. (1999). Mice lacking Smad3 show accelerated wound healing and an impaired local inflammatory response. *Nat. Cell Biol.* 1, 260–266.
- Ashcroft, G.S., Lei, K., Jin, W., Longenecker, G., Kulkarni, A.B., Greenwell-Wild, T., Hale-Donze, H., McGrady, G., Song, X.Y., and Wahl, S.M. (2000). Secretory leukocyte protease inhibitor mediates non-redundant functions necessary for normal wound healing. *Nat. Med.* 6, 1147–1153.
- Barrientos, S., Stojadinovic, O., Golinko, M.S., Brem, H., and Tomic-Canic, M. (2008). Growth factors and cytokines in wound healing. *Wound Repair Regen.* 16, 585–601.
- Bautista, D.M., Wilson, S.R., and Hoon, M.A. (2014). Why we scratch an itch: the molecules, cells and circuits of itch. *Nat. Neurosci.* 17, 175–182.
- Bilsborough, J., Mudri, S., Chadwick, E., Harder, B., and Dillon, S.R. (2010). IL-31 receptor (IL-31RA) knockout mice exhibit elevated responsiveness to oncostatin M. *J. Immunol.* 185, 6023–6030.
- Braiman-Wikman, L., Solomonik, I., Spira, R., and Tennenbaum, T. (2007). Novel insights into wound healing sequence of events. *Toxicol. Pathol.* 35, 767–779.
- Cevikbas, F., Wang, X., Akiyama, T., Kempkes, C., Savinko, T., Antal, A., Kukova, G., Buhl, T., Ikoma, A., Buddenkotte, J., et al. (2014). A sensory neuron-expressed IL-31 receptor mediates T helper cell-dependent itch: Involvement of TRPV1 and TRPA1. *J. Allergy Clin. Immunol.* 133, 448–460.
- Chavan, S.S., Pavlov, V.A., and Tracey, K.J. (2017). Mechanisms and Therapeutic Relevance of Neuro-immune Communication. *Immunity* 46, 927–942.
- Chen, W., Jin, W., Hardegen, N., Lei, K.J., Li, L., Marinos, N., McGrady, G., and Wahl, S.M. (2003). Conversion of peripheral CD4+CD25- naive T cells to CD4+CD25+ regulatory T cells by TGF-beta induction of transcription factor Foxp3. *J. Exp. Med.* 198, 1875–1886.
- Clausen, B.E., and Stoitzner, P. (2015). Functional Specialization of Skin Dendritic Cell Subsets in Regulating T Cell Responses. *Front. Immunol.* 6, 534.
- Colwell, A.S., Phan, T.T., Kong, W., Longaker, M.T., and Lorenz, P.H. (2005). Hypertrophic scar fibroblasts have increased connective tissue growth factor expression after transforming growth factor-beta stimulation. *Plast. Reconstr. Surg.* 116, 1387–1390, discussion 1391–1392.
- Cukjati, D., Rebersek, S., and Miklavcic, D. (2001). A reliable method of determining wound healing rate. *Med. Biol. Eng. Comput.* 39, 263–271.
- Dillon, S.R., Sprecher, C., Hammond, A., Bilsborough, J., Rosenfeld-Franklin, M., Presnell, S.R., Haugen, H.S., Maurer, M., Harder, B., Johnston, J., et al. (2004). Interleukin 31, a cytokine produced by activated T cells, induces dermatitis in mice. *Nat. Immunol.* 5, 752–760.
- Esebanmen, G.E., and Langridge, W.H.R. (2017). The role of TGF-beta signaling in dendritic cell tolerance. *Immunol. Res.* 65, 987–994.
- Feld, M., Garcia, R., Buddenkotte, J., Katayama, S., Lewis, K., Muirhead, G., Hevezi, P., Plessner, K., Schrupf, H., Krjutskov, K., et al. (2016). The pruritus- and TH2-associated cytokine IL-31 promotes growth of sensory nerves. *J. Allergy Clin. Immunol.* 138, 500–508.e24.
- Felker, P., Seré, K., Lin, Q., Becker, C., Hristov, M., Hieronymus, T., and Zenke, M. (2010). TGF-beta1 accelerates dendritic cell differentiation from common dendritic cell progenitors and directs subset specification toward conventional dendritic cells. *J. Immunol.* 185, 5326–5335.
- Guilliams, M., Crozat, K., Henri, S., Tamoutounour, S., Grenot, P., Devilard, E., de Bovis, B., Alexopoulou, L., Dalod, M., and Malissen, B. (2010). Skin-draining lymph nodes contain dermis-derived CD103(-) dendritic cells that constitutively produce retinoic acid and induce Foxp3(+) regulatory T cells. *Blood* 115, 1958–1968.
- Han, L., Ma, C., Liu, Q., Weng, H.J., Cui, Y., Tang, Z., Kim, Y., Nie, H., Qu, L., Patel, K.N., et al. (2013). A subpopulation of nociceptors specifically linked to itch. *Nat. Neurosci.* 16, 174–182.
- Hawro, T., Saluja, R., Weller, K., Altrichter, S., Metz, M., and Maurer, M. (2014). Interleukin-31 does not induce immediate itch in atopic dermatitis patients and healthy controls after skin challenge. *Allergy* 69, 113–117.
- Huang, J., Polgár, E., Solinski, H.J., Mishra, S.K., Tseng, P.Y., Iwagaki, N., Boyle, K.A., Dickie, A.C., Kriegbaum, M.C., Wildner, H., et al. (2018). Circuit dissection of the role of somatostatin in itch and pain. *Nat. Neurosci.* 21, 707–716.
- Imamachi, N., Park, G.H., Lee, H., Anderson, D.J., Simon, M.I., Basbaum, A.I., and Han, S.K. (2009). TRPV1-expressing primary afferents generate behavioral responses to pruritogens via multiple mechanisms. *Proc. Natl. Acad. Sci. USA* 106, 11330–11335.
- Jin, H., He, R., Oyoshi, M., and Geha, R.S. (2009). Animal models of atopic dermatitis. *J. Invest. Dermatol.* 129, 31–40.
- Kashem, S.W., Haniiffa, M., and Kaplan, D.H. (2017). Antigen-Presenting Cells in the Skin. *Annu. Rev. Immunol.* 35, 469–499.
- Kasutani, K., Fujii, E., Ohyama, S., Adachi, H., Hasegawa, M., Kitamura, H., and Yamashita, N. (2014). Anti-IL-31 receptor antibody is shown to be a potential therapeutic option for treating itch and dermatitis in mice. *Br. J. Pharmacol.* 171, 5049–5058.
- Keyes, B.E., Liu, S., Asare, A., Naik, S., Levorse, J., Polak, L., Lu, C.P., Nikolova, M., Pasolli, H.A., and Fuchs, E. (2016). Impaired Epidermal to Dendritic T Cell Signaling Slows Wound Repair in Aged Skin. *Cell* 167, 1323–1338.e14.
- Kissenpfennig, A., Henri, S., Dubois, B., Laplace-Builhé, C., Perrin, P., Romani, N., Tripp, C.H., Douillard, P., Leserman, L., Kaiserlian, D., et al. (2005). Dynamics and function of Langerhans cells in vivo: dermal dendritic cells colonize lymph node areas distinct from slower migrating Langerhans cells. *Immunity* 22, 643–654.
- Kitajima, M., and Ziegler, S.F. (2013). Cutting edge: identification of the thymic stromal lymphopoietin-responsive dendritic cell subset critical for initiation of type 2 contact hypersensitivity. *J. Immunol.* 191, 4903–4907.
- Lyman, I.R., Tenery, J.H., and Basson, R.P. (1970). Correlation between decrease in bacterial load and rate of wound healing. *Surg. Gynecol. Obstet.* 130, 616–621.
- Malissen, B., Tamoutounour, S., and Henri, S. (2014). The origins and functions of dendritic cells and macrophages in the skin. *Nat. Rev. Immunol.* 14, 417–428.
- Massagué, J. (1999). Wounding Smad. *Nat. Cell Biol.* 1, E117–E119.
- Mast, B.A., and Schultz, G.S. (1996). Interactions of cytokines, growth factors, and proteases in acute and chronic wounds. *Wound Repair Regen.* 4, 411–420.

- Meckmongkol, T.T., Harmon, R., McKeown-Longo, P., and Van De Water, L. (2007). The fibronectin synergy site modulates TGF-beta-dependent fibroblast contraction. *Biochem. Biophys. Res. Commun.* 360, 709–714.
- Meng, J., Moriyama, M., Feld, M., Buddenkotte, J., Buhl, T., Szollosi, A., Zhang, J., Miller, P., Ghetti, A., Fischer, M., et al. (2018). New mechanism underlying IL-31-induced atopic dermatitis. *J. Allergy Clin. Immunol.* 141, 1677–1689.e8.
- Meredith, M.M., Liu, K., Darrasse-Jeze, G., Kamphorst, A.O., Schreiber, H.A., Guermontprez, P., Idoyaga, J., Cheong, C., Yao, K.H., Niec, R.E., and Nussenzweig, M.C. (2012). Expression of the zinc finger transcription factor zDC (Zbtb46, Btbd4) defines the classical dendritic cell lineage. *J. Exp. Med.* 209, 1153–1165.
- Mishra, S.K., and Hoon, M.A. (2013). The cells and circuitry for itch responses in mice. *Science* 340, 968–971.
- Mishra, S.K., Tisel, S.M., Orestes, P., Bhargoo, S.K., and Hoon, M.A. (2011). TRPV1-lineage neurons are required for thermal sensation. *EMBO J.* 30, 582–593.
- Nattkemper, L.A., Tey, H.L., Valdes-Rodriguez, R., Lee, H., Mollanazar, N.K., Alborno, C., Sanders, K.M., and Yosipovitch, G. (2018). The Genetics of Chronic Itch: Gene Expression in the Skin of Patients with Atopic Dermatitis and Psoriasis with Severe Itch. *J. Invest. Dermatol.* 138, 1311–1317.
- Oetjen, L.K., Mack, M.R., Feng, J., Whelan, T.M., Niu, H., Guo, C.J., Chen, S., Trier, A.M., Xu, A.Z., Tripathi, S.V., et al. (2017). Sensory Neurons Co-opt Classical Immune Signaling Pathways to Mediate Chronic Itch. *Cell* 171, 217–228.e13.
- Parnell, L.K., Nedelec, B., Rachelska, G., and LaSalle, L. (2012). Assessment of pruritus characteristics and impact on burn survivors. *J. Burn Care Res.* 33, 407–418.
- Prasad, A., Thode, H.C., Jr., Sandoval, S., and Singer, A.J. (2019). The association of patient and burn characteristics with itching and pain severity. *Burns* 45, 348–353.
- Riol-Blanco, L., Ordovas-Montanes, J., Perro, M., Naval, E., Thiriot, A., Alvarez, D., Paust, S., Wood, J.N., and von Andrian, U.H. (2014). Nociceptive sensory neurons drive interleukin-23-mediated psoriasiform skin inflammation. *Nature* 510, 157–161.
- Ross, R., and Odland, G. (1968). Human wound repair. II. Inflammatory cells, epithelial-mesenchymal interrelations, and fibrogenesis. *J. Cell Biol.* 39, 152–168.
- Ruzicka, T., Hanifin, J.M., Furue, M., Pulka, G., Mlynarczyk, I., Wollenberg, A., Galus, R., Etoh, T., Mihara, R., Yoshida, H., et al.; XCIMA Study Group (2017). Anti-Interleukin-31 Receptor A Antibody for Atopic Dermatitis. *N. Engl. J. Med.* 376, 826–835.
- Schreiber, H.A., Loschko, J., Karssemeijer, R.A., Escolano, A., Meredith, M.M., Mucida, D., Guermontprez, P., and Nussenzweig, M.C. (2013). Intestinal monocytes and macrophages are required for T cell polarization in response to *Citrobacter rodentium*. *J. Exp. Med.* 210, 2025–2039.
- Shim, W.S., Tak, M.H., Lee, M.H., Kim, M., Kim, M., Koo, J.Y., Lee, C.H., Kim, M., and Oh, U. (2007). TRPV1 mediates histamine-induced itching via the activation of phospholipase A2 and 12-lipoxygenase. *J. Neurosci.* 27, 2331–2337.
- Shimada, S.G., and LaMotte, R.H. (2008). Behavioral differentiation between itch and pain in mouse. *Pain* 139, 681–687.
- Solinski, H.J., Dranchak, P., Oliphant, E., Gu, X., Earnest, T.W., Braisted, J., Inglese, J., and Hoon, M.A. (2019a). Inhibition of natriuretic peptide receptor 1 reduces itch in mice. *Sci. Transl. Med.* 11, eaav5464.
- Solinski, H.J., Kriegbaum, M.C., Tseng, P.Y., Earnest, T.W., Gu, X., Barik, A., Chesler, A.T., and Hoon, M.A. (2019b). Nppb Neurons Are Sensors of Mast Cell-Induced Itch. *Cell Rep.* 26, 3561–3573.e4.
- Steinhoff, M., Buddenkotte, J., and Lerner, E.A. (2018). Role of mast cells and basophils in pruritus. *Immunol. Rev.* 282, 248–264.
- Steward-Sharp, S.M., Laurence, A., Kanno, Y., Kotlyar, A., Villarino, A.V., Sciume, G., Kuchen, S., Resch, W., Wohlfert, E.A., Jiang, K., et al. (2014). A mouse model of HIES reveals pro- and anti-inflammatory functions of STAT3. *Blood* 123, 2978–2987.
- Takamori, A., Nambu, A., Sato, K., Yamaguchi, S., Matsuda, K., Numata, T., Sugawara, T., Yoshizaki, T., Arae, K., Morita, H., et al. (2018). IL-31 is crucial for induction of pruritus, but not inflammation, in contact hypersensitivity. *Sci. Rep.* 8, 6639.
- Tamoutounour, S., Guillems, M., Montanana Sanchis, F., Liu, H., Terhorst, D., Malosse, C., Pollet, E., Ardouin, L., Luche, H., Sanchez, C., et al. (2013). Origins and functional specialization of macrophages and of conventional and monocyte-derived dendritic cells in mouse skin. *Immunity* 39, 925–938.
- Tian, L., Rauvala, H., and Gahmberg, C.G. (2009). Neuronal regulation of immune responses in the central nervous system. *Trends Immunol.* 30, 91–99.
- Trier, A.M., and Kim, B.S. (2018). Cytokine modulation of atopic itch. *Curr. Opin. Immunol.* 54, 7–12.
- Tu, E., Chia, C.P.Z., Chen, W., Zhang, Y.E., Sun, L., and Chen, W. (2018). T Cell Receptor-Regulated TGF-beta Type I Receptor Expression Determines T Cell Quiescence and Activation. *Immunity* 48, 745–759.e6.
- Valladeau, J., and Saeland, S. (2005). Cutaneous dendritic cells. *Semin. Immunol.* 17, 273–283.
- van Duivenvoorde, L.M., van Mierlo, G.J., Boonman, Z.F., and Toes, R.E. (2006). Dendritic cells: vehicles for tolerance induction and prevention of autoimmune diseases. *Immunobiology* 211, 627–632.
- Wang, Z., Gao, Z., Shi, Y., Sun, Y., Lin, Z., Jiang, H., Hou, T., Wang, Q., Yuan, X., Zhu, X., et al. (2007). Inhibition of Smad3 expression decreases collagen synthesis in keloid disease fibroblasts. *J. Plast. Reconstr. Aesthet. Surg.* 60, 1193–1199.
- Yang, X., Letterio, J.J., Lechleider, R.J., Chen, L., Hayman, R., Gu, H., Roberts, A.B., and Deng, C. (1999). Targeted disruption of SMAD3 results in impaired mucosal immunity and diminished T cell responsiveness to TGF-beta. *EMBO J.* 18, 2180–2191.
- Zhang, Q., Putheti, P., Zhou, Q., Liu, Q., and Gao, W. (2008). Structures and biological functions of IL-31 and IL-31 receptors. *Cytokine Growth Factor Rev.* 19, 347–356.

STAR★METHODS

KEY RESOURCES TABLE

REAGENT or RESOURCE	SOURCE	IDENTIFIER
Antibodies		
Anti-mouse CD45 Alexa Fluor 700 (30-F11)	eBioscience	Cat# 56-0451-82; RRID:AB_891454
Anti-mouse CD3 PerCP-eFluor 710 (17A2)	eBioscience	Cat# 46-0032-82; RRID:AB_1834427
Anti-mouse CD3 APC-eFluor 780 (17A2)	eBioscience	Cat# 47-0032-82; RRID:AB_1272181
Anti-mouse CD11c PerCP/Cy5.5 (N418)	BioLegend	Cat# 117328; RRID:AB_2129641
Anti-mouse CD11c FITC (N418)	eBioscience	Cat# 11-0114-82; RRID:AB_464940
Anti-mouse CD11b APC (M1/70)	eBioscience	Cat# 17-0112-82; RRID:AB_469343
Anti-mouse CD11b eFluor 450 (M1/70)	eBioscience	Cat# 48-0112-82; RRID:AB_1582236
Anti-mouse CD326 APC (G8.8)	eBioscience	Cat# 17-5791-82; RRID:AB_2716944
Anti-mouse CD326 APC-eFluor 780 (G8.8)	eBioscience	Cat# 47-5791-82; RRID:AB_2573986
Anti-mouse CD64 PE-Cy7 (X54-5/7.1)	BioLegend	Cat# 139313; RRID:AB_2563903
Anti-mouse CD64 APC (X54-5/7.1)	eBioscience	Cat# 17-0641-82; RRID:AB_2735010
Anti-mouse CD64 PerCP-eFluor 710 (X54-5/7.1)	eBioscience	Cat# 46-0641-82; RRID:AB_2735016
Anti-mouse F4/80 APC (BM8)	eBioscience	Cat# 17-4801-82; RRID:AB_2784648
Anti-mouse F4/80 PE-eFluor 610 (BM8)	eBioscience	Cat# 61-4801-82; RRID:AB_2574612
Anti-mouse MHC class II (I-A/I-E) PE (M5/114.15.2)	eBioscience	Cat# 12-5321-82; RRID:AB_465928
Anti-mouse MHC class II (I-A/I-E) eFluor 450 (M5/114.15.2)	eBioscience	Cat# 48-5321-82; RRID:AB_1272204
Anti-mouse CD103 PE (2E7)	eBioscience	Cat# 12-1031-82; RRID:AB_465799
Anti-mouse CD207 PE (eBioL31)	eBioscience	Cat# 12-2075-82; RRID:AB_763452
Anti-mouse CD117 (2B8)	eBioscience	Cat# 48-1171-82; RRID:AB_2574037
Anti-mouse FcεR1 alpha PerCP-eFluor 710 (MAR-1)	eBioscience	Cat# 46-5898-82; RRID:AB_2573801
Anti-mouse Stat1	Cell Signaling	Cat# 9172; RRID:AB_2198300
Anti-mouse pStat1	Cell Signaling	Cat# 9171S; RRID:AB_331591
Anti-mouse Stat3	Cell Signaling	Cat# 9139; RRID:AB_331757
Anti-mouse Stat3	Cell Signaling	Cat# 4904S; RRID:AB_331269
Anti-mouse pStat3	Cell Signaling	Cat# 9131S; RRID:AB_331586
Anti-mouse pStat3	Cell Signaling	Cat# 9145S; RRID:AB_2491009
Anti-mouse Stat5	Cell Signaling	Cat# 9363; RRID:AB_2196923
Anti-mouse pStat5	Cell Signaling	Cat# 9351S; RRID:AB_2315225
Anti-mouse Gapdh	Cell Signaling	Cat# 5014S; RRID:AB_10693448
Anti-mouse IL-31	ABcam	Cat# ab102750; RRID:AB_10710722
TGF-β1 Elisa kit	Promega	Cat# G7591; RRID:AB_2858628
IL-31 Elisa kit	eBioscience	Cat# BMS6030; RRID:AB_2575653
Chemicals, Peptides, and Recombinant Proteins		
Recombinant mouse IL-1β	R&D System	Cat# 401-ML
Recombinant mouse IL-6	R&D System	Cat# 206-IL
Recombinant mouse IL-17a	R&D System	Cat# 421-ML
Recombinant mouse IL-31	R&D System	Cat# 3028-ML
Recombinant human TGF-β1	R&D System	Cat# 240-B
Recombinant mouse TNF-α	R&D System	Cat# 410-MT
SB431542	Selleckchem	Cat# S1067
S31-201	Sigma	Cat# SML0330
SIS3	Sigma	Cat# S0447
Capsaicin	Sigma	Cat# M2028

(Continued on next page)

Continued

REAGENT or RESOURCE	SOURCE	IDENTIFIER
poly-D-lysine	Sigma	Cat# A-003-M
Tamoxifen	Sigma	Cat# T5648
Liberase DH	Sigma	Cat# LIBDH-RO
Papain	Worthington	Cat# LS003127
Collagenase type II	Worthington	Cat# LS004177
Dispase type II	Worthington	Cat# LS02104
Fluo-4	Thermo Fisher Scientific	Cat# F14201
Pluronic F-127	Thermo Fisher Scientific	Cat# P3000MP
JS-11	Solinski et al., 2019a	N/A
Critical Commercial Assays		
RNeasy Mini Kit	QIAGEN	Cat# 74106
RNeasy Micro Kit	QIAGEN	Cat# 74004
High-Capacity cDNA Reverse Transcription Kit	Applied Biosystems	Cat# 4368814
TaqMan Gene Expression Master Mix	Applied Biosystems	Cat# 4369016
TaqMan PreAmp Master Mix Kit	Applied Biosystems	Cat# 4488593
Deposited Data		
Murine cutaneous wounds tissue RNA sequence data	This Paper	GEO accession GSE128193 https://www.ncbi.nlm.nih.gov/geo/query/acc.cgi?acc=GSE128193
Biological information		
Pruritus self-assessments of patients who were scheduled for minor skin superficial surgery were recorded before and every other day after surgery for 7 days, no human tissue sample was taken for this study	This Paper	N/A
Experimental Models: Organisms/Strains		
Mouse: C57BL/6	The Jackson Laboratory	Cat# 000664
Mouse: <i>Il31</i> ^{-/-}	Takamori et al., 2018	N/A
Mouse: <i>Trpv1</i> -cre	The Jackson Laboratory	Cat# 017769
Mouse: Rosa26 ^{tdTomato}	The Jackson Laboratory	Cat# 007914
Mouse: <i>Trpv1</i> -tdTomato	This paper	N/A
Mouse: mut-Stat3	The Jackson Laboratory	Cat# 027952
Mouse: zDC ^{DTR}	The Jackson Laboratory	Cat# 019506
Mouse: <i>Rag1</i> ^{-/-}	The Jackson Laboratory	Cat# 002216
Mouse: <i>Lang</i> ^{DTR}	The Jackson Laboratory	Cat# 016940
Mouse: <i>Csf1</i> ^{DTR}	The Jackson Laboratory	Cat# 024046
Mouse: <i>Csf1</i> ^{DTR} Lyz2-cre	Schreiber et al., 2013	N/A
Mouse: <i>Tgfb1</i> ^{+/+} Ert2-cre	Tu et al., 2018	N/A
Mouse: <i>Smad3</i> ^{-/-}	Yang et al., 1999	N/A
Mouse: <i>Tgfb1</i> ^{+/+} Cd11c-cre	This paper	N/A
Mouse: <i>Tgfb1</i> ^{+/+} Lyz2-cre	This paper	N/A
Oligonucleotides		
TaqMan <i>Hprt</i> primer, Mm00446968_m1	Applied Biosystems	N/A
TaqMan <i>Gapdh</i> primer, Mm99999915_g1	Applied Biosystems	N/A
TaqMan <i>Il31</i> primer, Mm01194496_m1	Applied Biosystems	N/A
TaqMan <i>Il31ra</i> primer, Mm01304494_m1	Applied Biosystems	N/A
TaqMan <i>Trpa1</i> primer, Mm01227437_m1	Applied Biosystems	N/A
TaqMan <i>Trpv1</i> primer, Mm01246302_m1	Applied Biosystems	N/A
TaqMan <i>Nppb</i> primer, Mm01255770_g1	Applied Biosystems	N/A

(Continued on next page)

Continued

REAGENT or RESOURCE	SOURCE	IDENTIFIER
Software and Algorithms		
FlowJo 9 software	FlowJo	https://www.flowjo.com ; RRID:SCR_008520
GraphPad Prism 7 software	GraphPad Software	https://www.graphpad.com ; RRID:SCR_002798
RStudio	RStudio	https://rstudio.com/ ; RRID:SCR_000432
Other		
BD LSRFortessa	BD Biosciences	N/A
BD FACSAria cell sorter	BD Biosciences	N/A

RESOURCE AVAILABILITY**Lead Contact**

Further information and requests for resources and reagents should be directed to and will be fulfilled by the Lead Contact, WanJun Chen (wchen@mail.nih.gov).

Materials Availability

This study did not generate new unique reagents

Data and Code Availability

Murine cutaneous wounds tissue RNA sequence data in this paper were deposited in GEO accession (GSE128193; <https://www.ncbi.nlm.nih.gov/geo/query/acc.cgi?acc=GSE128193>)

EXPERIMENTAL MODELS AND SUBJECT DETAILS**Human data of pruritus questionnaires**

The questionnaires for pruritus self-assessment was approved by the Institutional Ethics Committee of Beijing Stomatological Hospital affiliated to Capital Medical University; informed consent was obtained from all participants. Pruritus self-assessments were recorded for subjects who were scheduled for minor skin superficial surgery (please see [Method Details](#) for details). 12 subjects were enrolled finally (3 women and 9 men, mean age \pm SD: 53.3 \pm 12.6 years). Pruritus intensity was assessed using a 10-cm visual analog scale (VAS). Subjects were asked to evaluate and record the pruritus intensity before and every other day after surgery within 7 days. No human tissue sample was taken for this study.

Mice

C57BL/6, *Rag1*^{-/-} mice, *Trpv1*-Cre mice, *Rosa26*^{tdTomato} mice, *mut-Stat3* mice ([Steward-Tharp et al., 2014](#)), *zDC*^{DTR} mice ([Meredith et al., 2012](#)), *Csf1r*^{DTR} mice, *Lang*^{DTR} mice ([Kissenpfennig et al., 2005](#)) were obtained from The Jackson Laboratory. *Il31*^{-/-} mice ([Takamori et al., 2018](#)) were obtained from Dr. Nakae's Lab. *Tgfb1*^{1/1f} *Ert2*-Cre, *Smad3*^{-/-} (on a C57BL/6 background) were previously described and bred in our facility under specific pathogen-free conditions. *Trpv1*^{tdTomato} mice were generated in-house by crossing *Trpv1*-Cre mice with *Rosa26*^{tdTomato} mice. *Csf1r*^{DTR} *Lyz2*-Cre mice (MM^{DTR} mice) ([Schreiber et al., 2013](#)) were generated in-house by crossing *Lyz2*-Cre mice with *Csf1r*^{DTR} mice. *Tgfb1*^{1/1f} *Cd11c*-Cre⁺ mice were generated in-house by crossing *Cd11c*-Cre mice with *Tgfb1*^{1/1f} mice. *Tgfb1*^{1/1f} *Lyz2*-Cre⁺ were generated in-house by crossing *Lyz2*-Cre mice with *Tgfb1*^{1/1f} mice. *Tgfb1*^{1/1f} *Ert2*-Cre mice were treated with tamoxifen (1 μ g/mouse) per day for 5 days to delete T β RI. All mice used for experiments were aged 6-12 weeks, both male and female. All animal studies were performed according to National Institutes of Health (NIH) guidelines for use and care of live animals and approved by the Animal Care and Use Committees of National Institute of Dental and Craniofacial Research (NIDCR).

METHOD DETAILS**Enroll and exclusion criteria for human pruritus questionnaires**

All subjects must fulfill all the following items: (1) a superficial surgery is necessary for the subject diagnosed with a superficial cyst or benign tumor; (2) the expected wound will be 1 cm to 3 cm long; (3) the subject has no active systemic disease for 1 year and have a negative history of skin diseases; (4) the surgical area has no inflammation within the recent 6 months and have no sign of infection; (5) subject must be informed of the investigational nature of this study and given written informed consent. Exclusion criteria: (1) Active, uncontrolled infections in surgical area or systemically; (2) pathology report shows as a malignant tumor or Kimura's disease; (3) failed to follow up entirely.

Bone marrow chimeras and diphtheria toxin injection

C57BL/6 hosts were irradiated with 12Gy split into 3 doses and reconstituted by tail vein injection of 5×10^6 bone marrow cells from WT, $Il31^{-/-}$ or zDC^{DTR} donors. Mice were allowed to reconstitute for 6 weeks prior to use. Diphtheria toxin (DT) was purchased from Sigma-Aldrich. zDC^{DTR} bone marrow chimeras were injected *i.p.* with 20 ng DT per gram of body weight (500 ng/mouse) on the first day of DC depletion and with 4 ng DT per gram body weight (100 ng/mouse) on all subsequent days. C57BL/6, $Lang^{DTR}$, and MM^{DTR} mice received 4 ng DT per gram body weight (100 ng/mouse) at any time. Since we found that macrophage depletion at the beginning of incising would delay the wound healing or even fatal for mice, DT was injected (*i.p.*, 100ng/mouse) to MM^{DTR} mice on the 3rd of wound healing and every day thereafter.

Murine wound healing

Mice were anesthetized, dorsum shaved, cleaned with alcohol, and 2 equidistant 1cm full-thickness incisional wounds were made through the skin and left to heal. Wounds tissue (0.5 cm around incision) and dorsal root ganglion (DRG) that innervate the wound were harvested at indicated days and bisected for histology, snap-frozen in for RNA analysis/protein extraction, or DMEM contained 10% fetal bovine serum on ice for flow cytometry. Wound sizes were measured and wound healing rates were evaluated by the formula $((\pi/4) \times length_0 \times width_0 - (\pi/4) \times length_f \times width_f) / (day_f - day_0) \times ((\pi/4) \times length_0 \times width_0) \times 100$ (Cukjati et al., 2001; Lyman et al., 1970) and HE staining (Braiman-Wiksman et al., 2007).

IL-31 intradermal injection

For wound healing model, we intradermally injected IL-31 30 ng/site (by this dose IL-31 could not induce itch in naive mice 8 hours later; Arai et al., 2013) into wounds every 12 hours for 3 times from the fourth day after wounds were cut, and the behavior recordings were taken 8 hours after the last injection. For *mut-Stat3* mice or wild-type control mice, we injected IL-31 1 μ g/site on the dorsal area intradermally, and observe the itching behaviors 1 hour later; 8 hours after the 1st injection, another IL-31 injection (1 μ g/site, *i.d.*) on the same spot, itching behaviors were recorded again 1 hour after the 2nd injection.

Pruriceptive behavior measurement

To measure the pruriceptive behaviors, mice were placed in clear plastic enclosures with an optical cannula, which could rotate to allow free movement of the mouse. Itch behavioral responses were videotaped during the experiment. The behavior experiments and analysis were done blinded. Scratch (by the hind leg) bouts around the wounds or dendritic cells injected area were counted for 30 or 60 minutes.

RNA-seq analysis

Two wounds tissue from one animal were pooled, three animals were used per time point. The skin was cleaned of muscle and fat tissue; total RNA was extracted using the RNeasy mini kits (QIAGEN), purified using Direct-zol RNA MiniPrep kit (Zymo Research). Next-generation libraries were prepared using the VAHTS TM mRNA-seq V2 Library Prep Kit for Illumina (Vazyme, #NR601). RNA-seq libraries were run on an Illumina HiSeq X-Ten next-generation sequencer. Analysis of RNA-seq data was done using the DESeq package in R.

Cell culture of dorsal root ganglion neurons

Dorsal root ganglion (DRG) neurons were primarily cultured, as described previously. Briefly, thoracic and lumbar DRGs were dissected and collected from adult mice and transferred into HBSS without Ca^{2+}/Mg^{2+} on ice. F12 with 10% FCS and 100 U/ml penicillin/streptomycin was used as a culture medium. Ganglia were incubated with 1.5 mL papain (40 U/ml, Worthington) for 10 min at 37°C and then with 3 mL collagenase type II (4 mg/ml, Worthington)/ dispase type II (4.67 mg/ml, Worthington) combined solution for 10 min at 37°C. Dissociated cells were plated on poly-D-lysine-treated small coverslips and incubated for 2 to 3 days at 37°C in 95% air/5% CO₂.

Calcium image

DRG neurons were stained by 5 μ M Fluo-4 (Thermo Fisher Scientific) with 0.02% F-127 (Thermo Fisher Scientific) in HBSS^{+/+} RP free buffer at 37°C for 30 mins. Then coverslips with cells were washed, moved to a custom-built chamber, and incubated with image medium (pH 7.4; 140 mM NaCl, 5 mM KCl, 2 mM CaCl₂, 2 mM MgCl₂, 10 mM HEPES, 10 mM Glucose). Calcium imaging experiments were performed under a Nikon confocal microscope with 488 nm excitation wavelength. Neurons were stimulated by Capsaicin (50 nM, Sigma) 10 s after the time lapse started. Images were analyzed offline with an NIH ImageJ software, data were normalized by using the initial image as basal fluorescence, and presented as the relative change in fluorescence ($\Delta F/F_0$), where F_0 is basal fluorescence and $\Delta F = F - F_0$.

Flow cytometry

The skin was cleaned of fat tissue and cut into small pieces, incubated in Liberase DH (0.5 mg/ml, Sigma) for 90 min before finally shredding through 70- μ m cell strainers (BD Pharmingen). After isolation, cell suspensions were washed by 0.5% BSA in PBS and

passed through 40 μ m cell strainers (BD PharMingen), and cell populations were characterized by flow cytometry. Stained cells were analyzed on LSRIIFortessa (BD Biosciences) or separated by FACS Aria cell sorter (BD Biosciences). Data were analyzed with FlowJo software,

Dermal conventional type 2 dendritic cells culture and injection

Dermal conventional type 2 dendritic cells (cDC2) were sorted by FACS Aria cell sorter (Zombie⁻CD45⁺CD3⁻CD64⁻CD11c⁺CD326⁻CD11b⁺MHC II⁺) and cultured with complete medium (RPMI 1640 supplemented with 10% FBS, L-glutamine, penicillin/streptomycin, 2-mercaptoethanol) contained GM-CSF (20 ng/ml, Peprotech). For cDC2 injection, mice were dorsum shaved 1 day before injection, cDC2 were washed and suspended in HBSS^{+/+} RP free buffer and injected intradermally (5000 cells or 15000 cells in 20 μ L per site), pruriceptive behaviors were observed before and after injections.

Real-time PCR

Total RNA was derived from cultured cells with RNeasy Mini kits (QIAGEN) or RNeasy Micro kits (QIAGEN), cDNA was synthesized using a High Capacity cDNA Reverse Transcription kit (Applied Biosystems). For sorted cells, a TaqMan PreAmp Master Mix Kit (Applied Biosystems) was used before quantitative real-time PCR. Quantitative real-time PCR was performed according to the protocol of TaqMan gene expression assay kits (Applied Biosystems). Results from leukocytes were normalized to the expression of *Hprt* mRNA, results from tissue were normalized to the expression of *Gapdh* mRNA.

Antibodies and reagents

The following fluorochrome-conjugated antibodies were used for flow cytometry surface staining: anti-mouse CD45 (30-F11, eBioscience), anti-mouse CD3 (17A3, eBioscience), anti-mouse CD11c (N418, eBioscience), anti-mouse CD11b (M1/70, eBioscience), anti-mouse MHC class II (I-A/I-E) (M5/114.15.2, eBioscience), anti-mouse F4/80 (BM8, eBioscience), anti-mouse CD64 (X54-5/7.1, eBioscience), anti-mouse CD117 (2B8, eBioscience), anti-mouse Fc epsilon Receptor 1 alpha (MAR-1, eBioscience), anti-mouse CD207 (eBioL31, eBioscience), anti-mouse CD326 (G8.8, eBioscience), anti-mouse CD103 (2E7, eBioscience). Dead cells were excluded from analysis using Zombie Yellow Fixable Viability Kit (Biolegend). Recombined proteins and chemicals: IL-1 β (401-ML, R&D System), IL-6 (206-IL, R&D System), IL-17a (421-ML, R&D System), IL-31 (3028-ML, R&D System), TGF- β 1 (240-B, R&D System), TNF- α (410-MT, R&D System), SB431542 (ALK5 inhibitor, Selleckchem), S3I-201 (Stat3 inhibitor, Selleckchem), and SIS3 (Smad3 inhibitor, Sigma) were used in cell culturing for different conditions. Anti-mouse Stat1 (#9172, Cell Signaling), anti-mouse pStat1 (#9171S, Cell Signaling), anti-mouse Stat3 (#9139, Cell Signaling), anti-mouse pStat3 (#9131S, Cell Signaling), anti-mouse Stat5 (#9363, Cell Signaling), anti-mouse pStat5 (#9351S, Cell Signaling), anti-mouse Gapdh (#5014S, Cell Signaling), anti-mouse IL-31 (ab102750, Abcam) were used for western blot. TGF β 1 Elisa kit (G7591, Promega) and IL-31 Elisa kit (BMS6030, eBioscience) were used for TGF β 1 or IL-31 protein determination.

Statistical analysis

Statistical analysis was performed using either unpaired two-tailed Student's *t* tests or one-way ANOVA in GraphPad Prism.



Since January 2020 Elsevier has created a COVID-19 resource centre with free information in English and Mandarin on the novel coronavirus COVID-19. The COVID-19 resource centre is hosted on Elsevier Connect, the company's public news and information website.

Elsevier hereby grants permission to make all its COVID-19-related research that is available on the COVID-19 resource centre - including this research content - immediately available in PubMed Central and other publicly funded repositories, such as the WHO COVID database with rights for unrestricted research re-use and analyses in any form or by any means with acknowledgement of the original source. These permissions are granted for free by Elsevier for as long as the COVID-19 resource centre remains active.

RESEARCH

Open Access



A novel murine model of combined hepatocellular carcinoma and intrahepatic cholangiocarcinoma

Ru-Chen Xu^{1,2†}, Fu Wang^{1,2†}, Jia-Lei Sun^{1,2}, Weinire Abuduwalli^{1,2}, Guang-Cong Zhang^{1,2}, Zhi-Yong Liu^{1,2}, Tao-Tao Liu^{1,2}, Ling Dong^{1,2}, Xi-Zhong Shen^{1,2,3} and Ji-Min Zhu^{1,2*} 

Abstract

Primary liver cancer (PLC) is a common gastrointestinal malignancy worldwide. While hepatocellular carcinoma (HCC) and intrahepatic cholangiocarcinoma (ICC) are two major pathologic types of PLC, combined HCC and ICC (cHCC-ICC) is a relatively rare subtype that shares both hepatocyte and cholangiocyte differentiation. However, the molecular feature of this unique tumor remains elusive because of its low incidence and lack of a suitable animal model. Herein, we generated a novel spontaneous cHCC-ICC model using a Sleeping Beauty-dependent transposon plasmid co-expressing oncogenic *Myc* and *AKT1* and a CRISPR-Cas9 plasmid expressing single-guide RNA targeting *p53* into mouse hepatocytes via in situ electroporation. The histological and transcriptional analysis confirmed that this model exhibits cHCC-ICC features and activates pathways committing cHCC-ICC formation, such as TGF- β , WNT, and NF- κ B. Using this model, we further screened and identified LAMB1, a protein involved in cell adhesion and migration, as a potential therapeutic target for cHCC-ICC. In conclusion, our work presents a novel genetic cHCC-ICC model and provides new insights into cHCC-ICC.

Keywords: *Myc*, *AKT1*, *p53*, LAMB1, Sleeping Beauty-dependent transposon system, In situ electroporation

Introduction

Primary liver cancer (PLC), including hepatocellular carcinoma (HCC) and intrahepatic cholangiocarcinoma (ICC), represents the third cause of cancer-related death [1, 2]. Research has revealed that ICC and HCC share a monoclonal origin with bidirectional phenotype differentiation and may appear simultaneously [3]. Combined HCC and ICC (cHCC-ICC) is a rare tumor accounting for 0.4–14.2% of all PLC [4–7]. Since the diagnosis of cHCC-ICC relies on evidence of histological findings and patients who are not suitable for resection may be

misdiagnosed with HCC or ICC alone, the actual incidence underestimates the current cHCC-ICC burden [5]. Although curative surgical resection or liver transplantation is considered the mainstay of clinical practice, up to 80% of patients relapse within 5 years due to lymph node metastasis and vascular invasion [8, 9]. Unfortunately, the 5-year survival in patients with unresectable cHCC-ICC does not exceed 30% due to inadequate response to current treatments [10, 11]. Taking these findings into account when making treatment decisions, a more focused understanding of the molecular pathology and identification of potential therapeutic targets of cHCC-ICC thus are urgently needed.

Compared to xenograft tumor models, genetically engineered tumor models develop *de novo* tumors that closely imitate the histopathological features of their human counterparts [12]. Hydrodynamic tail vein

[†]Ru-Chen Xu and Fu Wang contributed equally to this work

*Correspondence: zhu.jimin@zs-hospital.sh.cn

¹ Department of Gastroenterology and Hepatology, Zhongshan Hospital of Fudan University, 180 Fenglin Rd., Shanghai 200032, China
Full list of author information is available at the end of the article



© The Author(s) 2022. **Open Access** This article is licensed under a Creative Commons Attribution 4.0 International License, which permits use, sharing, adaptation, distribution and reproduction in any medium or format, as long as you give appropriate credit to the original author(s) and the source, provide a link to the Creative Commons licence, and indicate if changes were made. The images or other third party material in this article are included in the article's Creative Commons licence, unless indicated otherwise in a credit line to the material. If material is not included in the article's Creative Commons licence and your intended use is not permitted by statutory regulation or exceeds the permitted use, you will need to obtain permission directly from the copyright holder. To view a copy of this licence, visit <http://creativecommons.org/licenses/by/4.0/>. The Creative Commons Public Domain Dedication waiver (<http://creativecommons.org/publicdomain/zero/1.0/>) applies to the data made available in this article, unless otherwise stated in a credit line to the data.

injection (HDVI) and in situ electroporation (Epo) are two ways to transfer foreign plasmid DNA directly into hepatocytes. HDVI can create a pressurized blood force that redirects the blood flow directly into the liver, leading to plasmid DNA entering the intracellular compartment of hepatocytes [13], while electroporation is an efficient way to introduce foreign genes into cultured cells and able to in situ transfer plasmids into hepatocytes [14].

Recently, high-throughput genomic studies have revealed a series of driver genes contributing to HCC or ICC tumorigenesis [15, 16]. *c-Myc* and *TP53* are two top frequently mutated genes in HCC patients. Recently, co-delivery of *c-Myc*-encoding plasmid and CRISPR/Cas9-mediated *p53* knockout via HDVI successfully developed spontaneous HCC in mice [17, 18]. In another study, Seehawer M et al. constructed a vector that co-expressed *Myc* and *AKT1* to establish HCC in *p19Arf*^{-/-} mice via HDVI [19]. Interestingly, the same vector led to ICC tumorigenesis by the approach of Epo, which could cause in situ necroptosis microenvironment, highlighting the hepatic microenvironment may contribute to lineage commitment during tumorigenesis [19].

In the current study, we applied a Sleeping Beauty-dependent transposon plasmid co-expressing oncogenic *Myc* and *AKT1* in combination with a CRISPR-Cas9 plasmid expressing single-guide RNA targeting *p53* to compare their tumorigenic capacity via either HDVI- or Epo-dependent hepatocyte delivery. Notably, we found transfection of these plasmids by Epo led to the cHCC-ICC formation. Taking advantage of this novel spontaneous model, we proposed that LAMB1 may serve as a therapeutic target for cHCC-ICC.

Materials and methods

Vectors

A plasmid that co-expressing oncogenic *Myc* and *AKT1* was a kind gift and has been constructed and described previously [19]. The SB13 transposase-encoding vector was kindly provided by Dr Yue Zhao. pX330 backbone expressing sgRNA targeting *p53* was obtained from Tyler Jacks (Addgene plasmid #59910).

Animal studies

Male 4 to 6-week-old C57BL/6J mice were purchased from Charles River (Shanghai, China), and all the animals used in the study were fed in a specific pathogen-free facility. All animal care and experimental protocols were approved by the Institutional Animal Care and Use Committee (IACUC) of Zhongshan Hospital, Fudan University.

Hydrodynamic tail vein injection and in situ electroporation

For hydrodynamic tail vein injection, 30 µg *Myc* + *AKT1* co-expressing plasmid, 30 µg pX330 sg-*p53* plasmid, and 10 µg SB13 transposase-encoding plasmid were prepared in 2 ml of sterile PBS and injected into a tail vein within 3–5 s per mouse. For in situ electroporation, 6-week-old wild-type C57BL/6J mice were anesthetized, and the right lateral liver lobe was exposed after midline laparotomy. Plasmids described above were resolved in 50 µg sterile PBS and injected into the right lateral liver lobe using an insulin needle. In situ electroporation was performed with Squaare Wave Electroporator (Nepa Gene). The voltage and duration of electric pulse were 70 V and 75 ms, respectively. Two pulses were applied, and the interval was 500 ms.

Immunohistochemistry

Immunohistochemistry (IHC) was performed as previously described [20]. In brief, the sections of tumors were incubated with the following antibodies: HNF4α (ab201460, Abcam), CK-19 (ab52625, Abcam), PCNA (2586, Cell Signaling Technology), p-AKT (Ser473, 4060, Cell Signaling Technology), p-ERK (Thr202/Tyr204, 4370, Cell Signaling Technology), p-NF-κB (Ser536, 3033, Cell Signaling Technology), β-catenin (8480, Cell Signaling Technology), TGF-β (21898-1-AP, Proteintech) and FGFR2 (13042-1-AP, Proteintech).

RNA-sequencing and analysis

RNA-sequencing for whole transcriptome analysis was performed using Illumina NovaSeq 6000 platform according to the manufacturer's protocol. Three biological replicates were applied for RNA-seq, and all RNA samples passed quality control with 5–8 Gb and Q20 ≥ 90. Hierarchical clustering of RNA-seq was performed using R language with the 'pheatmap' package. A Euclidean method was used to calculate distance measurements, while the 'complete' method was utilized to calculate the dissimilarity values for hierarchical clustering. For the heatmap visualization, gene expression values were normalized.

Bioinformatic analysis

Gene set enrichment analysis (GSEA) was performed using GSEA software version 4.1.0 with 1,000 permutations of the gene sets. The FPKM values from the RNA-seq were compared against the specific gene sets. Gene sets used in this study were downloaded from the

MSigdb database (<http://software.broadinstitute.org/gsea/msigdb/index.jsp>).

Statistics

The statistical analysis was performed using Prism Graphpad 7.0 software. Quantitative variables were analyzed by paired *t*-test. Kaplan-Meier analysis was used to compare OS between HDVI and Epo groups. Data were presented as mean \pm standard deviation. $p < 0.05$ was considered statistically significant.

Results

Generation of spontaneous liver cancer model through HDVI and Epo

Myc, *AKT1*, and *TP53* are among the top frequent mutated genes in PLC. To assess their roles in liver cancer tumorigenesis, a vector expressing constitutively active oncogenic *Myc* and *AKT1*, and single-guild RNA targeting *TP53* (sgTp53) was transfected into mouse liver cells based on a Sleeping Beauty (SB) transposon system via either HDVI or Epo (Fig. 1A, B). Both methods induced liver cancer 3–4 weeks after vector delivery, showing

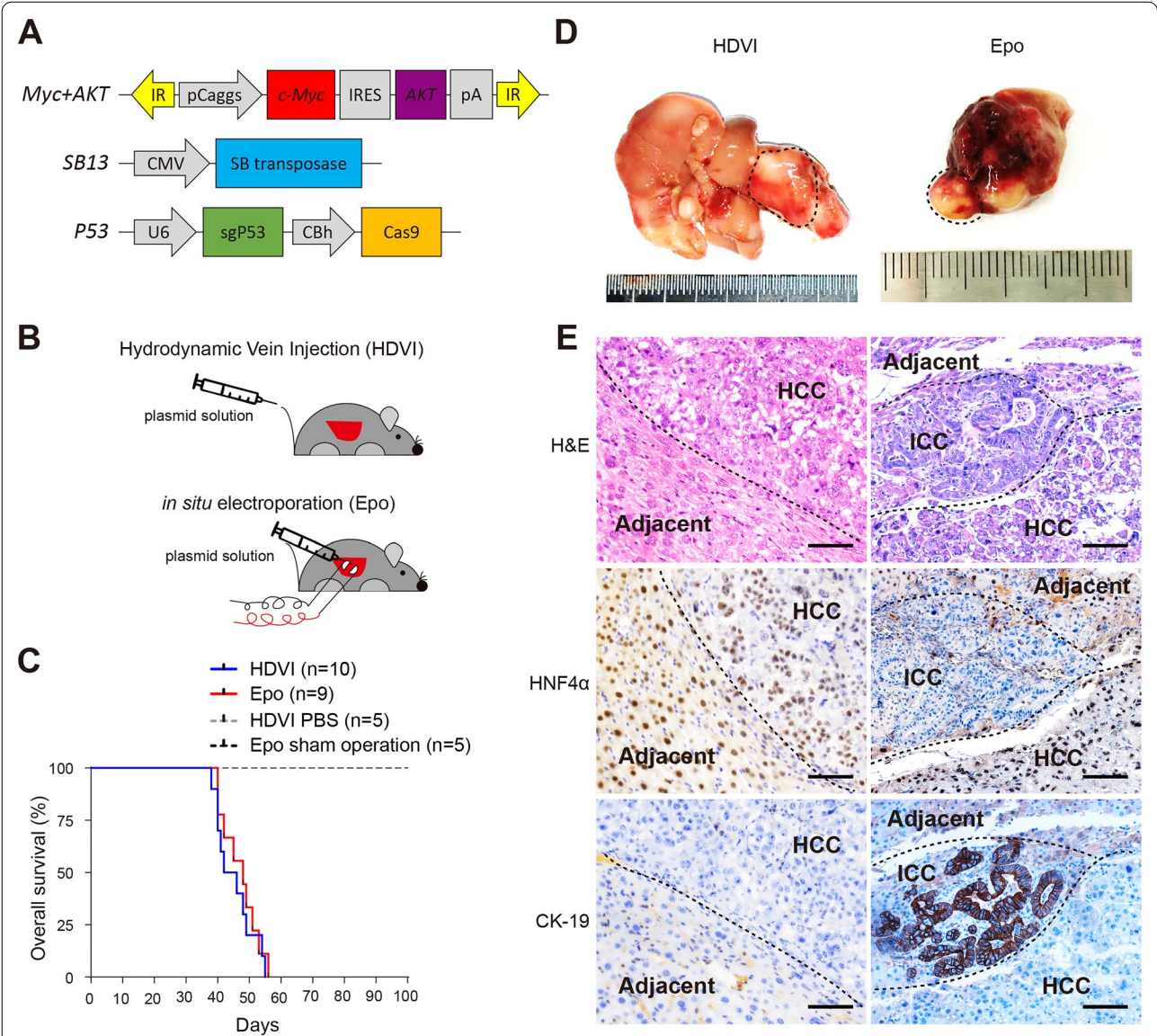


Fig. 1 Generation of spontaneous primary liver cancer model using hydrodynamic tail vein injection (HDVI) and in situ electroporation (Epo). **A** Schematic of plasmids designed. **B** Schematic of intrahepatic delivery of plasmids through HDVI or Epo. **C** The overall survival rate of *MAPHDVI* and *MAPEpo* mice, respectively. **D** Representative images of livers from mice received HDVI- or Epo-dependent plasmids via intrahepatic transfection. **E** Representative hematoxylin and eosin (H&E), HNF4α, and CK-19 staining of liver tissues shown in Fig. 1D. Scale bar, 200 μm

comparable overall survival rates (Fig. 1C). Tumors generated by HDVI (termed as *MAPHDVI*) exhibited multifocal neoplasia, while tumors generated by Epo (termed as *MAPEpo*) exhibited a unilocular pattern (Fig. 1D). H&E staining revealed disorderly and mitotically activated epithelial cells with abnormal pleomorphic nuclei and loss of polarity in all *MAPHDVI* tumors (Fig. 1E). Also, bile duct-like tissues were observed in *MAPEpo* tumors rather than in *MAPHDVI* tumors (Fig. 1E). IHC staining confirmed that *MAPHDVI* were HCC, as evidenced by solid nuclear staining for hepatocyte nuclear factor 4- α (HNF4 α), a liver-specific marker, but negative staining for cytokeratin 19 (CK-19), a marker of biliary differentiation. Interestingly, staining of both HNF4 α and CK-19 in *MAPEpo* tumors with a clear boundary confirmed a combined HCC and ICC within the same tumor (Fig. 1E). These data indicate that induction of *Myc* and *AKT1* and loss of *TP53* by HDVI lead to spontaneous HCC formation while Epo leads to cHCC-ICC.

Transcriptional analysis of the *MAPHDVI* and *MAPEpo* tumors

To further validate the morphological findings, RNA-seq analysis for *MAPHDVI* and *MAPEpo* was performed to investigate the transcriptome differences. Tumor tissues from *MAPHDVI* and *MAPEpo*, along with normal liver tissue from wild-type C57BL/6J mice as control, were firstly assessed for hepatocyte and biliary differentiation markers. The results suggested that *MAPHDVI* tumors exhibited higher expression of hepatic markers, including *Afp*, *Alb*, *Adh1*, *Hnf4a*, *Onecut1*, *F2*, *Aldob*, and *Fabp1*. However, genes involved in biliary differentiation, including *Krt19*, *Krt7*, *Ehf*, *Gprc5a*, *Nes*, *Tgfb1*, *Tgfb2*, and *Jag1*, were highly expressed in *MAPEpo* tumors but not in *MAPHDVI* tumors [21] (Fig. 2A). Further GESA analysis confirmed that liver-specific gene signature was significantly enriched in normal liver tissues and *MAPHDVI* tumors rather than in *MAPEpo* tumors (Fig. 1B). A previous study transcriptionally profiled 20 cHCC-ICC

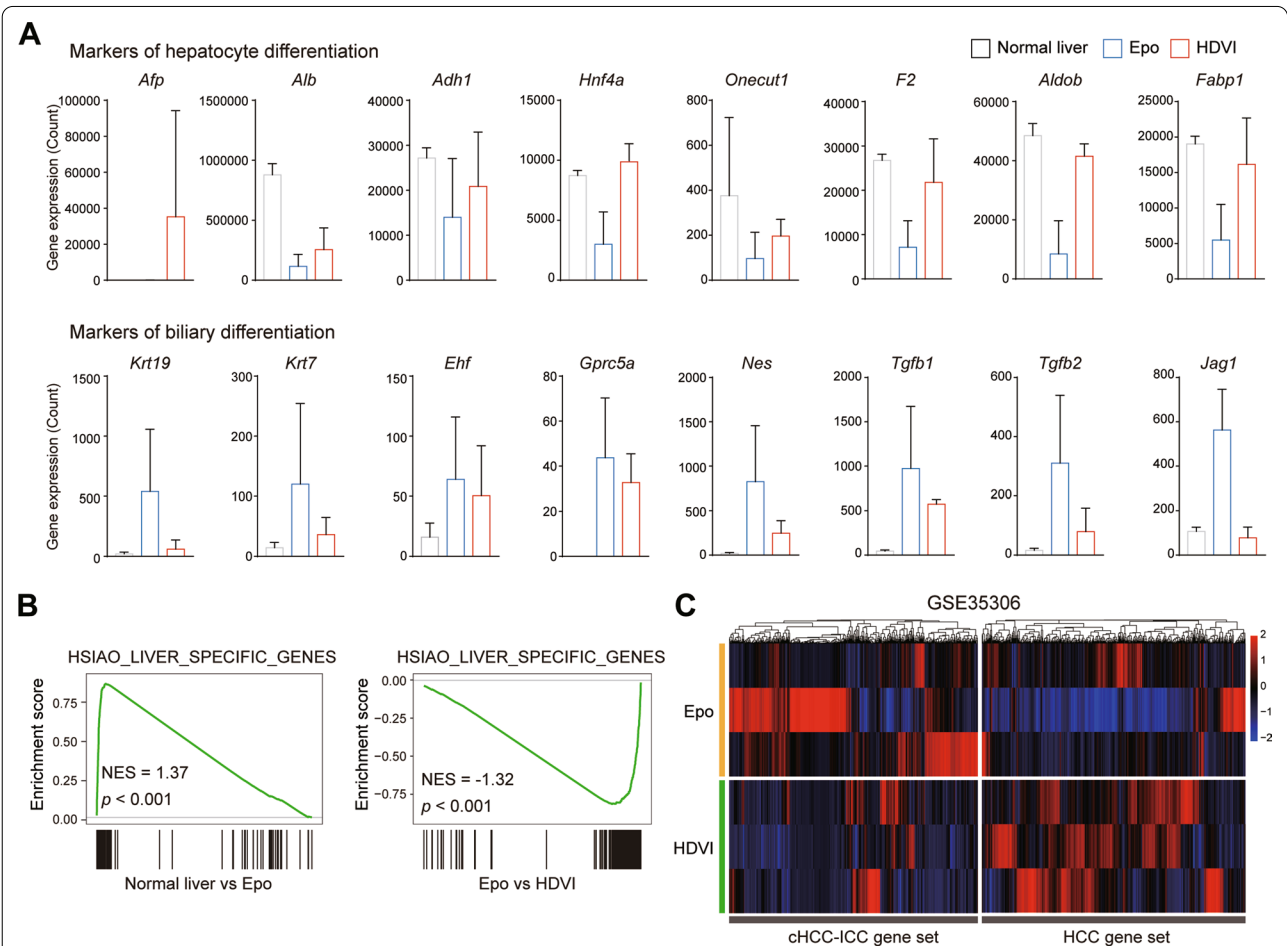


Fig. 2 Transcriptome analysis of *MAPHDVI* and *MAPEpo* tumors. **A** Expression of genes that involves in hepatocyte and biliary differentiation. **B** GESA analysis using transcriptome profiles of *MAPHDVI* and *MAPEpo* tumors. Enrichment plots were presented for liver-specific gene signature. **C** Hierarchal clustering analysis of HCC- and cHCC-ICC-related genes was performed in *MAPHDVI* and *MAPEpo* tumors

and successfully identified a series of gene sets that could represent cHCC-ICC and HCC genome features [22]. cHCC-ICC-related gene set comprised 588 up-regulated genes, while the HCC-related gene set contained 656 up-regulated genes. Using these gene sets, Hierarchical clustering analysis revealed that *MAPEpo* tumors had higher expression of genes associated with cHCC-ICC. In contrast, *MAPHDVI* tumors had higher expression of genes involved in HCC. Collectively, these transcriptome data further support the successful generation of spontaneous cHCC-ICC through *Epo*.

Signaling pathways that commit cHCC-ICC activates in *MAPEpo* tumors

Several key signaling pathways, including the AKT, RAS, NF- κ B, WNT- β -catenin, and TGF- β signaling pathways, have been identified as responsible for initiating and developing cHCC-ICC [23]. We, therefore, examined whether these pathways were also activated in the *MAPEpo* model. GSEA analysis proved that genes in the RAS, NF- κ B, WNT, and TGF- β signaling pathways were significantly enriched in *MAPEpo* tumors rather than in normal liver tissues (Fig. 3A). Although the enrichment score produced no statistical discrepancy, these pathways tended to be relatively enriched in *MAPEpo* tumor rather than in *MAPHDVI* tumor, probably because of the mixed HCC and ICC within the tumor (Fig. 3A). IHC analysis for HCC and ICC components was subsequently performed in *MAPEpo* tumors to dissect this phenotype better. A comparable PCNA staining pattern among *MAPHDVI*, HCC-*MAPEpo*, and ICC-*MAPEpo* tumors was observed, suggesting a similar proliferation in these tumor cells (Fig. 3B). Notably, IHC staining was strongly positive for p-AKT, p-ERK, p-NF- κ B, β -catenin, and TGF- β in the ICC component of the *MAPEpo* tumors, where FGFR2 served as the positive control (Fig. 3B). Taken together, these data suggest that the signaling pathways that contributed to cHCC-ICC formation and development are activated in *MAPEpo* tumors.

Identification of LAMB1 may serve as a potential therapy target for cHCC-ICC

As our preliminary data implied that *MAPEpo* tumor resembled human cHCC-ICC, we, therefore, utilized this model to explore its clinical relevance. Differentially expressed genes ($\text{Log}_2\text{FC} \geq 1$ or ≤ -1 , $p < 0.05$) between *MAPEpo* tumor and *MAPHDVI* tumor were profiled to find genes involved in cHCC-ICC but not in HCC. The results indicated that 552 genes were overexpressed while 568 genes were downregulated in *MAPEpo* tumor compared to that in *MAPHDVI* (Fig. 4A). To further verify the consistency of our findings, previously reported upregulated genes in cHCC-ICC and upregulated genes

in *MAPEpo* tumors were compared. A total of 73 overlapping genes were identified (Fig. 4B).

Using these overlapping genes as input, Gene Ontology analysis revealed that biological processes (BP) were mainly enriched in tumor metastasis-related changes such as extracellular matrix organization (ECM), cell adhesion, and cell migration (Fig. 4C). Kyoto Encyclopedia of Genes and Genomes (KEGG) analysis demonstrated that focal adhesion and ECM-receptor interaction were among the top two pathways enriched (Fig. 4D). These results were consistent with the invasive feature of cHCC-ICC.

In the 73 overlapping genes, *Lamb1*, which contributes to ECM activity and cell adhesion and is highly expressed in cHCC-ICC, was identified. We also found that *LAMB1* expression in human cHCC-ICC (GSE35306) was significantly higher than in both ICC and HCC tissues. For further validation, we analyzed another two published datasets (GSE84073 and GSE15765) that contain transcriptome data of human ICC, HCC, and cHCC-ICC. It also exhibited that *LAMB1* was upregulated in human cHCC-ICC compared with HCC (Fig. 4E). Considering minimal data on cHCC-ICC are available, no significant changes of *Lamb1* were observed between cHCC-ICC and ICC. To sum up, these findings imply that *Lamb1* may serve as a therapeutic target for cHCC-ICC, and further study is needed to dissect its role in cHCC-ICC.

Discussion

cHCC-ICC is a rare type of PLC but has attracted increasing attention in recent years. Because the diagnosis of cHCC-ICC largely depends on histochemistry, the true incidence of cHCC-ICC is likely to be underestimated, making the knowledge and management of cHCC-ICC inaccessible. Thus, a tumor animal model that resembles clinical cHCC-ICC is essential for further investigation. In this study, we generated a spontaneous cHCC-ICC by induction of oncogenic *Myc* and *AKT1* and loss of *p53* through in situ electroporation. Evidence showed that this model shared similar transcriptome and oncogenic signaling pathways with human cHCC-ICC. Most importantly, we, for the first time, identified *LAMB1* as a potential therapy target for cHCC-ICC.

Most solid tumors, especially HCC, develop in the context of chronic diseases and are composed of heterogeneous malignant cells. Importantly, the heterogeneous feature of tumor cells is a key reason for clinical drug resistance. Although traditional syngeneic or xenograft models are easy to perform, these models are unable to fully mimic specific human disease conditions and neglect the heterogeneous feature of tumor tissues. Thus, these common models have a limit to evaluating the drugs pre-clinically. It is well known that tumor cells

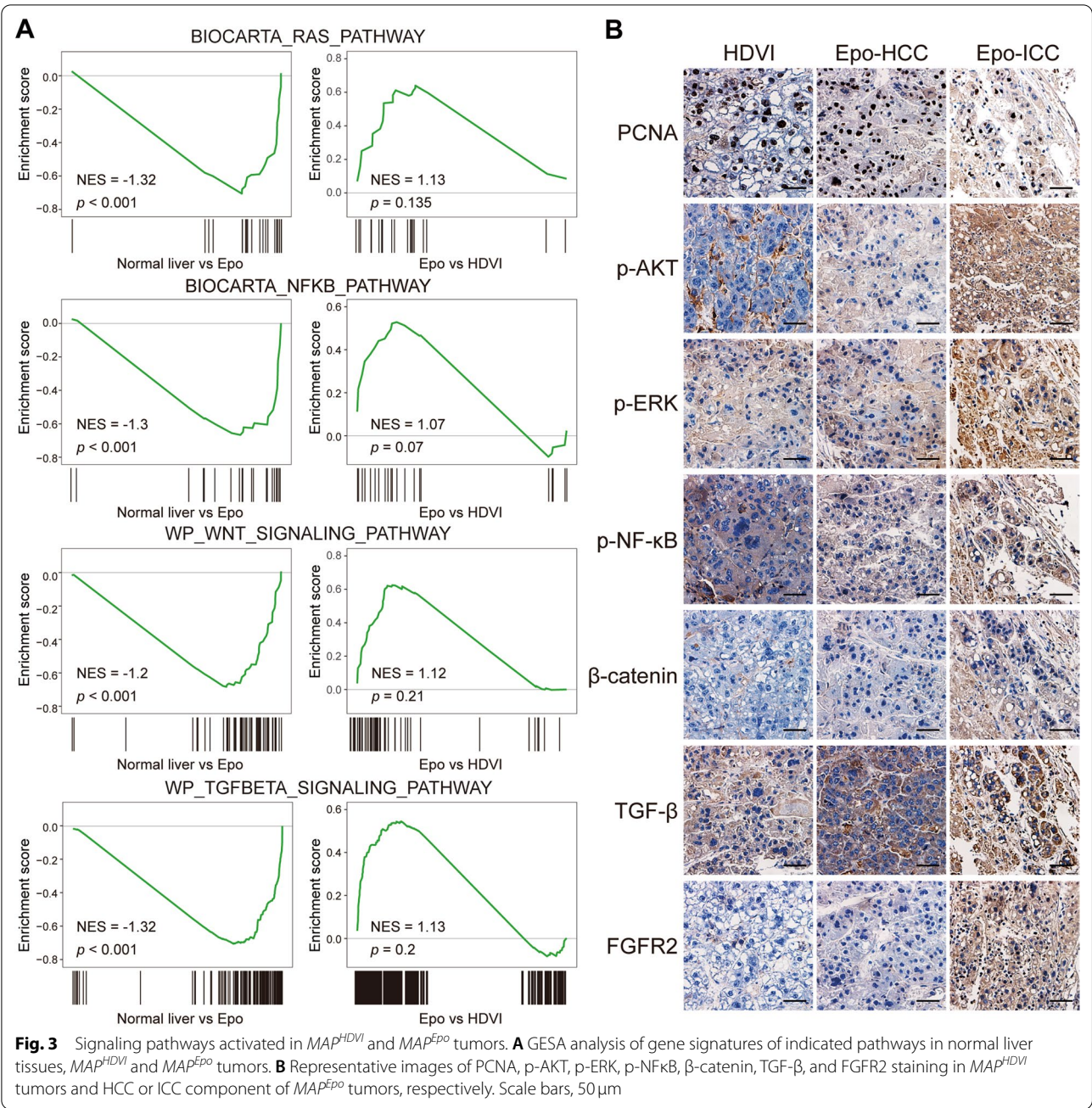
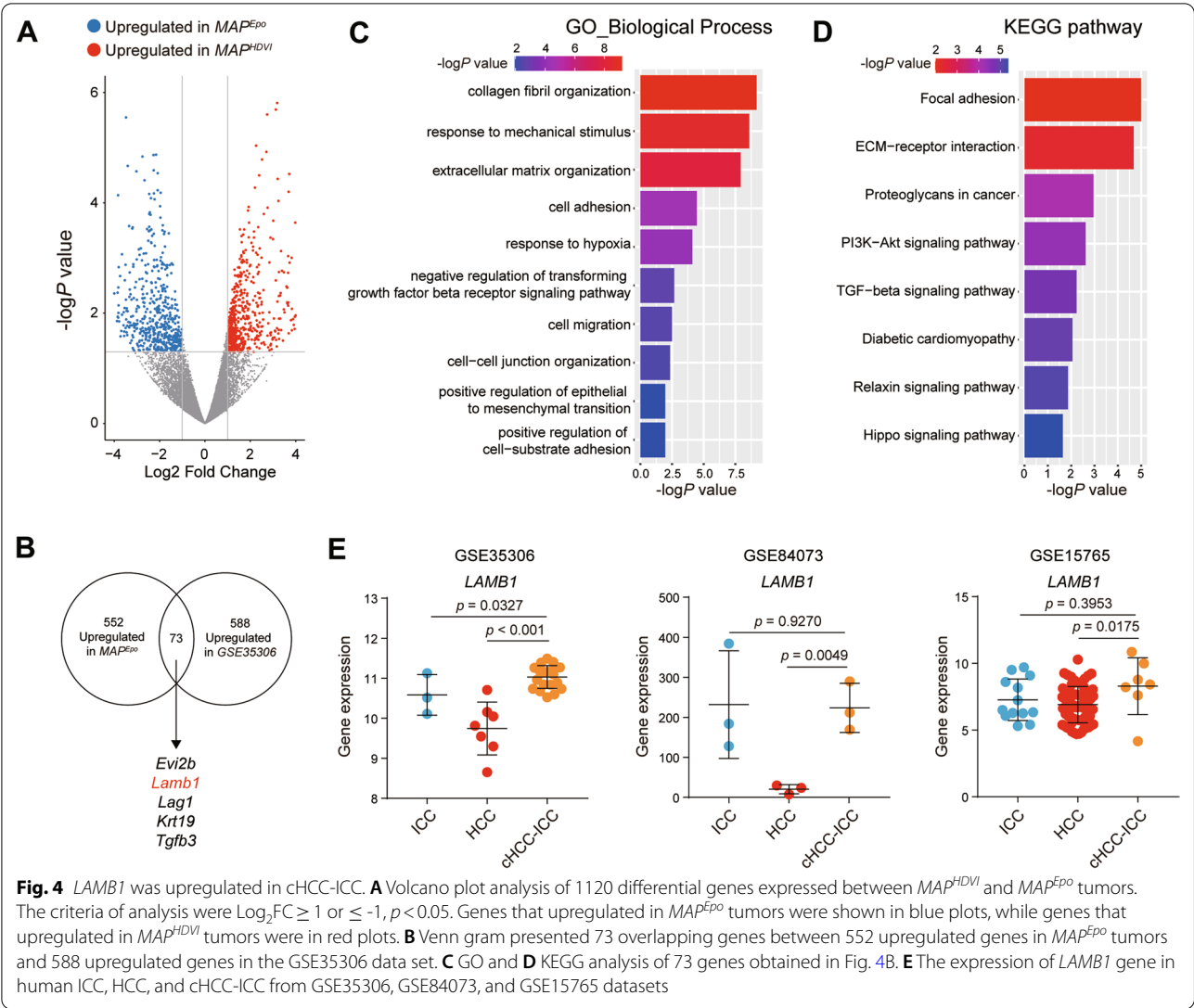


Fig. 3 Signaling pathways activated in MAP^{HDVI} and MAP^{Epo} tumors. **A** GSEA analysis of gene signatures of indicated pathways in normal liver tissues, MAP^{HDVI} and MAP^{Epo} tumors. **B** Representative images of PCNA, p-AKT, p-ERK, p-NF-kB, β-catenin, TGF-β, and FGFR2 staining in MAP^{HDVI} tumors and HCC or ICC component of MAP^{Epo} tumors, respectively. Scale bars, 50 μm

are transformed from normal cells carrying oncogenic mutations, making it possible to induce PLC by genetic engineering. Accumulative studies have revealed specific mutations that lead to either HCC or ICC tumorigenesis. For example, *c-Myc*, *CTNNB1* and *TP53* are among top mutated genes for HCC patients [24]; while *KRAS*, a powerful oncogene involved in glandular malignant, is able to induce ICC when specifically expressed in mouse hepatocytes [25]. Currently, genetic engineered mouse model (GEMM) is an ideal tool for study HCC or ICC

tumorigenesis and has clear genetic background resembling human disease, making it suitable for pre-clinical estimation. Unfortunately, few studies focus on cHCC-ICC as it's not entirely clear how cHCC-ICC occurs. A recent study proved that an inflammatory tumor microenvironment directs lineage commitment of the PLC [19]. Here, we used electroporation to induce a necrotic liver microenvironment and established cHCC-ICC formation by combining *Myc* and *AKT1* knockin with *p53* knockout. The morphological and genetic evidences



proved successful induction of cHCC-ICC. Our work provides a simple GEMM for cHCC-ICC with direct clinical translational value. However, our study also has limitations. It remains elusive whether other gene combinations can lead to the cHCC-ICC formation in the same experimental setting. Moreover, our model does not exhibit the metastatic feature of cHCC-ICC, as evidenced by no lung metastatic lesion observed (data not shown). New gene combinations that can lead to metastasis should be tested in the future.

Whether cHCC-ICC is a unique or a subtype of HCC or ICC has long been controversial. cHCC-ICC can be further divided into three subtypes according to Allen and Lisa's criteria that are separate type (HCC and ICC components physically separated), combined type (HCC and ICC component in the same tumor with clear boundaries), and mixed type (HCC and ICC component in the same tumor with no boundaries) [26]. Histologically, we found that *MAPEpo* tumors exhibited features with a combined type of cHCC-ICC. Recently, Xue et al. [3] comprehensively analyzed a total of 133 cHCC-ICC cases and revealed that combined type of cHCC-ICC acquired intense ICC-like landscapes, including high expression of *KRT19* but a lower expression of HCC markers (including *AFP* and *GPC3*), which is also supported by our transcriptome data (Fig. 2A). Compared with *MAPHDVI* tumors, *MAPEpo* tumors tended to express markers of biliary differentiation, especially for *Krt19*, *Krt7*, *Nes*, *Tgfb2*, and *Jag1*. Consistently, *Afp* expression is much higher in *MAPHDVI* tumors than in *MAPEpo* tumors. These data suggested that *MAPEpo* tumors might exhibit more ICC-like characteristics.

Despite apparent molecular discrepancy among subtypes of cHCC-ICC, they all have poorer prognosis and

more invasive features than HCC and are similar to ICC [27]. Interactions between cell adhesion or migration and ECM are vital factors that mediate tumor metastasis. In our study, we identified 73 overlapping genes that are highly upregulated in cHCC-ICC. Bioinformatic analysis indicated that these genes were mainly involved in ECM bioprocesses and cell adhesion. These findings further reinforced the invasive feature of cHCC-ICC.

Laminins, a family of extracellular matrix glycoproteins, are among the predominant component of ECM [28]. Evidence reported that laminins participated in tumor metastasis by promoting cell adhesion and migration, and their receptors expressed on the tumor cell surface [29–31]. We screened these 73 genes and identified a main differential gene *Lamb1*, a member of the laminin family. Taking advantage of several data sets reported previously, we established that *Lamb1* was upregulated in cHCC-ICC compared to HCC, but its expression seemed comparable with ICC. It has been reported that LAMB1 overexpressed in several types of tumors and correlated with tumor metastasis and poor prognosis [32–34]. The prognosis value of LAMB1 was further screened in TCGA database. The results suggested that LAMB1 is elevated in a series of tumors, but LAMB1 is negatively correlated with both OS and DFS for LIHC, CHOL, and COAD (Additional file 1: Fig. S1). Most importantly, KEGG and GSEA analysis showed that LAMB1 played a pivotal role in pro-metastatic processes, including focal adhesion, ECM-receptor interaction, and cellular junction in LIHC, CHOL, and COAD, highlighting that LAMB1 might also be a potential treating target for cHCC-ICC (Additional file 1: Fig. S2). Since clinical transcriptome data of patients with cHCC-ICC remains very limited, we were able only to verify the expression of *Lamb1* in current published data; further larger-scale studies should be performed to assess its clinical value. Summarily, the present study established a human-resembling cHCC-ICC model via in situ electroporation. This novel preclinical model can be used to investigate the molecular feature of cHCC-ICC.

Supplementary Information

The online version contains supplementary material available at <https://doi.org/10.1186/s12967-022-03791-z>.

Additional file 1. Figure S1. Multi-cancer analysis of the expression and prognostic role of LAMB1. **A** LAMB1 is significantly upregulated in multiple cancer types from TCGA data. **B** Kaplan-Meier analysis of the association between LAMB1 expression and OS or DFS in LIHC, CHOL, and COAD datasets. **Figure S2.** Multi-cancer analysis of biological functions and significant pathway of LAMB1. **A** Top 20 pathways enriched in the KEGG analysis in LIHC, CHOL, and COAD datasets. The red box represents pro-metastatic processes, including focal adhesion, ECM-receptor interaction, and cellular junction. **B** GSEA analysis of gene signatures of indicated pathways in LIHC, CHOL, and COAD datasets.

Acknowledgements

Not applicable.

Author contributions

Concept, drafting and interpretation: RCX, FW, and JMZ. Execution and analysis: RCX, FW, JLS, WA, GCZ, ZYL, TTL, LD, XZS, and JMZ. All authors contributed to the article and approved the submitted version. All authors read and approved the final manuscript.

Funding

This study was partly supported by the National Natural Science Foundation of China (No. 81472673, and No. 81672720).

Availability of data and materials

The datasets used and analyzed during the current study are available from the corresponding author on reasonable request.

Declarations

Ethics approval and consent to participate

All animal experiments were approved by the Animal Ethics and Welfare Committee of Zhongshan Hospital, Fudan University.

Consent for publication

All authors have approved the manuscript for submission.

Competing interests

The authors declare that they have no competing interests.

Author details

¹Department of Gastroenterology and Hepatology, Zhongshan Hospital of Fudan University, 180 Fenglin Rd., Shanghai 200032, China. ²Shanghai Institute of Liver Diseases, Shanghai, China. ³Key Laboratory of Medical Molecular Virology, Shanghai Medical College of Fudan University, Shanghai, China.

Received: 16 August 2022 Accepted: 24 November 2022

Published online: 09 December 2022

References

- Sung H, Ferlay J, Siegel RL, Laversanne M, Soerjomataram I, Jemal A, Bray F. Global Cancer Statistics 2020: GLOBOCAN estimates of incidence and Mortality Worldwide for 36 cancers in 185 countries. *CA Cancer J Clin*. 2021;71:209–49.
- Zhou J, Sun H, Wang Z, Cong W, Wang J, Zeng M, Zhou W, Bie P, Liu L, Wen T, et al. Guidelines for the diagnosis and treatment of hepatocellular carcinoma (2019 Edition). *Liver Cancer*. 2020;9:682–720.
- Xue R, Chen L, Zhang C, Fujita M, Li R, Yan SM, Ong CK, Liao X, Gao Q, Sasagawa S, et al. Genomic and transcriptomic profiling of combined hepatocellular and intrahepatic cholangiocarcinoma reveals distinct molecular subtypes. *Cancer Cell*. 2019;35:932–47.e938.
- Ramai D, Ofosu A, Lai JK, Reddy M, Adler DG. Combined hepatocellular cholangiocarcinoma: a population-based retrospective study. *Am J Gastroenterol*. 2019;114:1496–501.
- Garancini M, Goffredo P, Pagni F, Romano F, Roman S, Sosa JA, Giardini V. Combined hepatocellular-cholangiocarcinoma: a population-level analysis of an uncommon primary liver tumor. *Liver Transpl*. 2014;20:952–9.
- Jarnagin WR, Weber S, Tickoo SK, Koea JB, Obiekwe S, Fong Y, DeMatteo RP, Blumgart LH, Klimstra D. Combined hepatocellular and cholangiocarcinoma: demographic, clinical, and prognostic factors. *Cancer*. 2002;94:2040–6.
- Lee CC, Wu CY, Chen JT, Chen GH. Comparing combined hepatocellular-cholangiocarcinoma and cholangiocarcinoma: a clinicopathological study. *Hepatogastroenterology*. 2002;49:1487–90.
- Yoon YI, Hwang S, Lee YJ, Kim KH, Ahn CS, Moon DB, Ha TY, Song GW, Jung DH, Lee JW, et al. Postresection outcomes of combined hepatocellular carcinoma-cholangiocarcinoma, hepatocellular carcinoma and intrahepatic cholangiocarcinoma. *J Gastrointest Surg*. 2016;20:411–20.

9. Yin X, Zhang BH, Qiu SJ, Ren ZG, Zhou J, Chen XH, Zhou Y, Fan J. Combined hepatocellular carcinoma and cholangiocarcinoma: clinical features, treatment modalities, and prognosis. *Ann Surg Oncol*. 2012;19:2869–76.
10. Yamashita YI, Aishima S, Nakao Y, Yoshizumi T, Nagano H, Kuroki T, Takami Y, Ide T, Ohta M, Takatsuki M, et al. Clinicopathological characteristics of combined hepatocellular cholangiocarcinoma from the viewpoint of patient prognosis after hepatic resection: high rate of early recurrence and its predictors. *Hepatol Res*. 2020;50:863–70.
11. Magistri P, Tarantino G, Serra V, Guidetti C, Ballarin R, Di Benedetto F. Liver transplantation and combined hepatocellular-cholangiocarcinoma: feasibility and outcomes. *Dig Liver Dis*. 2017;49:467–70.
12. Brown ZJ, Heinrich B, Greten TF. Mouse models of hepatocellular carcinoma: an overview and highlights for immunotherapy research. *Nat Rev Gastroenterol Hepatol*. 2018;15:536–54.
13. Chen X, Calvisi DF. Hydrodynamic transfection for generation of novel mouse models for liver cancer research. *Am J Pathol*. 2014;184:912–23.
14. Suzuki T, Shin BC, Fujikura K, Matsuzaki T, Takata K. Direct gene transfer into rat liver cells by in vivo electroporation. *FEBS Lett*. 1998;425:436–40.
15. Dong LQ, Shi Y, Ma LJ, Yang LX, Wang XY, Zhang S, Wang ZC, Duan M, Zhang Z, Liu LZ, et al. Spatial and temporal clonal evolution of intrahepatic cholangiocarcinoma. *J Hepatol*. 2018;69:89–98.
16. Gao Q, Zhu H, Dong L, Shi W, Chen R, Song Z, Huang C, Li J, Dong X, Zhou Y, et al. Integrated proteogenomic characterization of HBV-related hepatocellular carcinoma. *Cell*. 2019;179:561–77.e522.
17. Ruiz de Galarreta M, Bresnahan E, Molina-Sánchez P, Lindblad KE, Maier B, Sia D, Puigvehi M, Miquela V, Casanova-Acebes M, Dhainaut M, et al. β -Catenin activation promotes Immune escape and resistance to Anti-PD-1 therapy in hepatocellular carcinoma. *Cancer Discov*. 2019;9:1124–41.
18. Hu B, Yu M, Ma X, Sun J, Liu C, Wang C, Wu S, Fu P, Yang Z, He Y, et al. IFN α potentiates Anti-PD-1 efficacy by remodeling glucose metabolism in the hepatocellular carcinoma microenvironment. *Cancer Discov*. 2022;12:1718–41.
19. Seehawer M, Heinzmann F, D'Artista L, Harbig J, Roux PF, Hoenicke L, Dang H, Klotz S, Robinson L, Dore G, et al. Necroptosis microenvironment directs lineage commitment in liver cancer. *Nature*. 2018;562:69–75.
20. Sun J, Zhou C, Zhao Y, Zhang X, Chen W, Zhou Q, Hu B, Gao D, Raatz L, Wang Z, et al. Quiescin sulfhydryl oxidase 1 promotes sorafenib-induced ferroptosis in hepatocellular carcinoma by driving EGFR endosomal trafficking and inhibiting NRF2 activation. *Redox Biol*. 2021;41:101942.
21. Lin YK, Fang Z, Jiang TY, Wan ZH, Pan YF, Ma YH, Shi YY, Tan YX, Dong LW, Zhang YJ, Wang HY. Combination of Kras activation and PTEN deletion contributes to murine hepatopancreatic ductal malignancy. *Cancer Lett*. 2018;421:161–9.
22. Coulouarn C, Cavard C, Rubbia-Brandt L, Audebourg A, Dumont F, Jacques S, Just PA, Clément B, Gilgenkrantz H, Perret C, Terris B. Combined hepatocellular-cholangiocarcinomas exhibit progenitor features and activation of wnt and TGF β signaling pathways. *Carcinogenesis*. 2012;33:1791–6.
23. Wang G, Wang Q, Liang N, Xue H, Yang T, Chen X, Qiu Z, Zeng C, Sun T, Yuan W, et al. Oncogenic driver genes and tumor microenvironment determine the type of liver cancer. *Cell Death Dis*. 2020;11:313.
24. Friemel J, Frick L, Unger K, Egger M, Parrotta R, Boge YT, Adili A, Karin M, Luedde T, Heikenwalder M, Weber A. Characterization of HCC Mouse Models: towards an etiology-oriented Subtyping Approach. *Mol Cancer Res*. 2019;17:1493–502.
25. Tanaka M, Kunita A, Yamagishi M, Katoh H, Ishikawa S, Yamamoto H, Abe J, Arita J, Hasegawa K, Shibata T, Ushiku T. KRAS mutation in intrahepatic cholangiocarcinoma: linkage with metastasis-free survival and reduced E-cadherin expression. *Liver Int*. 2022;42:2329–40.
26. Allen RA, Lisa JR. Combined liver cell and bile duct carcinoma. *Am J Pathol*. 1949;25:647–55.
27. Wakizaka K, Yokoo H, Kamiyama T, Ohira M, Kato K, Fujii Y, Sugiyama K, Okada N, Ohata T, Nagatsu A, et al. Clinical and pathological features of combined hepatocellular-cholangiocarcinoma compared with other liver cancers. *J Gastroenterol Hepatol*. 2019;34:1074–80.
28. Patarroyo M, Tryggvason K, Virtanen I. Laminin isoforms in tumor invasion, angiogenesis and metastasis. *Semin Cancer Biol*. 2002;12:197–207.
29. Liang Y, Chen X, Wu Y, Li J, Zhang S, Wang K, Guan X, Yang K, Bai Y. LncRNA CASC9 promotes esophageal squamous cell carcinoma metastasis through upregulating LAMC2 expression by interacting with the CREB-binding protein. *Cell Death Differ*. 2018;25:1980–95.
30. Dai J, Cimino PJ, Gouin KH, Grzelak CA, Barrett A, Lim AR, Long A, Weaver S, Saldin LT, Uzamere A, et al. Astrocytic laminin-211 drives disseminated breast tumor cell dormancy in brain. *Nat Cancer*. 2022;3:25–42.
31. Reuten R, Zendeheroud S, Nicolau M, Fleischhauer L, Laitala A, Kiderlen S, Nikodemus D, Wullkopf L, Nielsen SR, McNeilly S, et al. Basement membrane stiffness determines metastases formation. *Nat Mater*. 2021;20:892–903.
32. Shan H, Liu T, Gan H, He S, Deng J, Hu X, Li L, Cai L, He J, Long H, et al. RNA helicase DDX24 stabilizes LAMB1 to promote hepatocellular carcinoma progression. *Cancer Res*. 2022. <https://doi.org/10.1158/0008-5472.CAN-21-3748>.
33. Chen Z, Yang X, Bi G, Liang J, Hu Z, Zhao M, Li M, Lu T, Zheng Y, Sui Q, et al. Ligand-receptor interaction atlas within and between tumor cells and T cells in lung adenocarcinoma. *Int J Biol Sci*. 2020;16:2205–19.
34. Meves A, Nikolova E, Heim JB, Squirewell EJ, Cappel MA, Pittelkow MR, Otley CC, Behrendt N, Saunte DM, Lock-Andersen J, et al. Tumor cell adhesion as a risk factor for sentinel lymph node metastasis in primary cutaneous melanoma. *J Clin Oncol*. 2015;33:2509–15.

Publisher's Note

Springer Nature remains neutral with regard to jurisdictional claims in published maps and institutional affiliations.

Ready to submit your research? Choose BMC and benefit from:

- fast, convenient online submission
- thorough peer review by experienced researchers in your field
- rapid publication on acceptance
- support for research data, including large and complex data types
- gold Open Access which fosters wider collaboration and increased citations
- maximum visibility for your research: over 100M website views per year

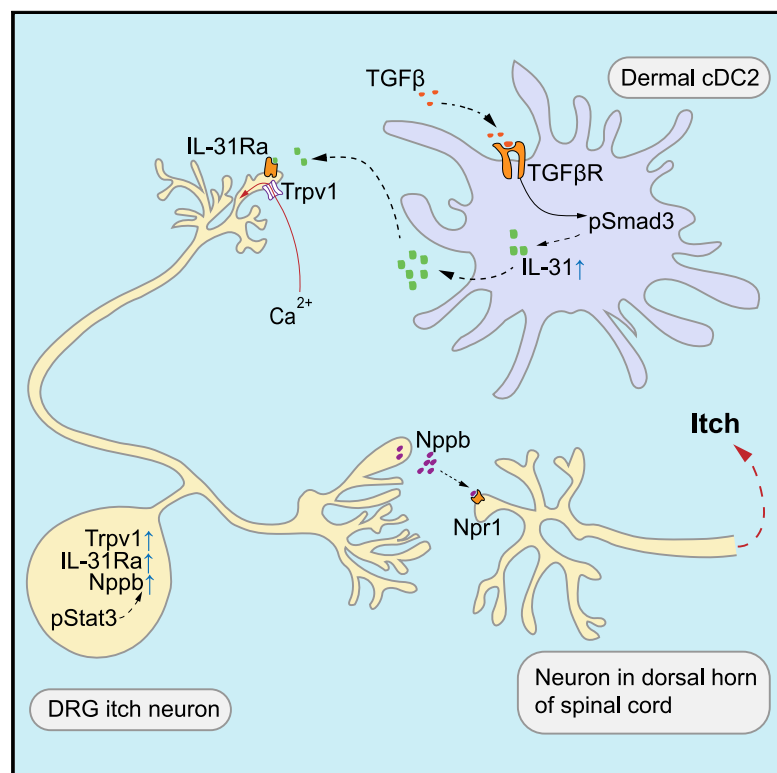
At BMC, research is always in progress.

Learn more biomedcentral.com/submissions



The Cytokine TGF- β Induces Interleukin-31 Expression from Dermal Dendritic Cells to Activate Sensory Neurons and Stimulate Wound Itching

Graphical Abstract



Authors

Junji Xu, Peter Zanvit, Lei Hu, ...,
Mark A. Hoon, Songlin Wang,
WanJun Chen

Correspondence

wchen@mail.nih.gov

In Brief

Xu et al. find that TGF- β , produced as part of the wound healing process, induces expression of interleukin-31 by dermal conventional type 2 DCs, which, in turn, increases neuron sensitivity and provokes itching.

Highlights

- IL-31 expression is increased in skin wounds during the peak of itch response
- *Il31*^{-/-} mice have less itch behavior during wound healing
- IL-31 increases calcium influx and *Il31ra*, *Trpv1* expression in itch sensory neurons
- TGF- β 1 induces expression of IL-31 in dermal conventional type 2 dendritic cells



Xu et al., 2020, Immunity 53, 371–383
August 18, 2020 Published by Elsevier Inc.
<https://doi.org/10.1016/j.immuni.2020.06.023>

八.材料9.其他科研能力和综合水平的证明材料

- (1) 发明专利:
- (2) 软件专利著作

(1) 实用新型专利



(2) 软著



九.材料 11.攻读博士学位的研究计划书

攻读博士学位期间拟开展的研究计划

一、已取得的主要研究成果：

目前共发表了5篇SCI论文，目录如下：

1. *in*
im 21;
9(2
2. *s a*
Bio and
Met
3. **J** *rg.*
202
4. *Q.*
Dia for
tub **IF:**
3.3
5. *L,*
Wa all
cell *nn*
Tra

二、博士学位期间拟开展研究课题：

1. 拟开展研究的课题名称：

课题名称（中）：胸水可溶性 Fas 配体对结核性胸腔积液的诊断价值

课题名称（英）：Diagnostic value of soluble Fas ligand in pleural fluid for tuberculous pleural effusion

2. 拟开展研究课题的国内外研究现状及选题意义:

结核性胸腔积液的诊断现状

TPE 的诊断手段[9]。

结核性胸腔积液生化标志物的研究现状

学
发
干
国
并
作
受

生化标志物，以弥补 ADA 的不足，或将其取代[11, 19]。

胸水中可溶性 Fas 配体是十分有潜质的 TPE 诊断标志物

F

约 40

活 ca

(sFas

sFasL

(i) sFa

因胸

我们

的思 ， 一 。

参考文献

1. P. Tian, R. Qiu, M. Wang, et al. Prevalence, Causes, and Health Care Burden of Pleural Effusions Among Hospitalized Adults in China. *JAMA Netw Open*. 2021; 4(8): e2120306. <http://doi.org/10.1001/jamanetworkopen.2021.20306>.
2. J.M. Porcel, A. Esquerda, M. Vives, S. Bielsa. Etiology of pleural effusions: analysis of more than 3,000 consecutive thoracenteses. *Arch Bronconeumol*. 2014; 50(5): 161-5. <http://doi.org/10.1016/j.arbres.2013.11.007>.
3. S. Bielsa, C. Acosta, M. Pardina, C. Civit, J.M. Porcel. Tuberculous Pleural Effusion: Clinical Characteristics of 320 Patients. *Arch Bronconeumol*. 2019; 55(1): 17-22. <http://doi.org/10.1016/j.arbres.2018.04.014>.
4. M. Zhang, D. Li, Z.D. Hu, Y.L. Huang. The diagnostic utility of pleural markers for tuberculosis pleural effusion. *Ann Transl Med*. 2020; 8(9): 607. <http://doi.org/10.21037/atm.2019.09.110>.
5. M. Kohli, I. Schiller, N. Dendukuri, et al. Xpert((R)) MTB/RIF assay for extrapulmonary tuberculosis and rifampicin resistance. *Cochrane Database Syst Rev*. 2018; 8: CD012768. <http://doi.org/10.1002/14651858.CD012768.pub2>.
6. I.S. Sehgal, S. Dhooria, A.N. Aggarwal, D. Behera, R. Agarwal. Diagnostic Performance of Xpert MTB/RIF in Tuberculous Pleural Effusion: Systematic Review and Meta-analysis. *J Clin Microbiol*. 2016; 54(4): 1133-6. <http://doi.org/10.1128/jcm.03205-15>.
7. X.J. Wang, Y. Yang, Z. Wang, et al. Efficacy and safety of diagnostic thoracoscopy in undiagnosed pleural effusions. *Respiration*. 2015; 90(3): 251-5. <http://doi.org/10.1159/000435962>.
8. Y. Wei, K. Shen, T. Lv, et al. Comparison between closed pleural biopsy and medical thoracoscopy for the diagnosis of undiagnosed exudative pleural effusions: a systematic

- review and meta-analysis. *Transl Lung Cancer Res.* 2020; 9(3): 446-58. <http://doi.org/10.21037/tlcr.2020.03.28>.
9. Q. Zhou, Y.Q. Chen, S.M. Qin, et al. Diagnostic accuracy of T-cell interferon-gamma release assays in tuberculous pleurisy: a meta-analysis. *Respirology.* 2011; 16(3): 473-80. <http://doi.org/10.1111/j.1440-1843.2011.01941.x>.
10. J.M. Porcel. Advances in the diagnosis of tuberculous pleuritis. *Ann Transl Med.* 2016; 4(15): 282. <http://doi.org/10.21037/atm.2016.07.23>.
11. J.M. Porcel. Biomarkers in the diagnosis of pleural diseases: a 2018 update. *Ther Adv Respir Dis.* 2018; 12: 1753466618808660. <http://doi.org/10.1177/1753466618808660>.
12. W. Wang, Q. Zhou, K. Zhai, et al. Diagnostic accuracy of interleukin 27 for tuberculous pleural effusion: two prospective studies and one meta-analysis. *Thorax.* 2018; 73(3): 240-7. <http://doi.org/10.1136/thoraxjnl-2016-209718>.
13. J. Jiang, H.Z. Shi, Q.L. Liang, S.M. Qin, X.J. Qin. Diagnostic value of interferon-gamma in tuberculous pleurisy: a metaanalysis. *Chest.* 2007; 131(4): 1133-41. <http://doi.org/10.1378/chest.06-2273>.
14. Q.L. Liang, H.Z. Shi, K. Wang, S.M. Qin, X.J. Qin. Diagnostic accuracy of adenosine deaminase in tuberculous pleurisy: a meta-analysis. *Respir Med.* 2008; 102(5): 744-54. <http://doi.org/10.1016/j.rmed.2007.12.007>.
15. C. Hooper, Y.C. Lee, N. Maskell, B.T.S.P.G. Group. Investigation of a unilateral pleural effusion in adults: British Thoracic Society Pleural Disease Guideline 2010. *Thorax.* 2010; 65 Suppl 2: ii4-17. <http://doi.org/10.1136/thx.2010.136978>.
16. A.N. Aggarwal, R. Agarwal, S. Dhooria, et al. Comparative accuracy of pleural fluid unstimulated interferon-gamma and adenosine deaminase for diagnosing pleural tuberculosis: A systematic review and meta-analysis. *PLoS One.* 2021; 16(6): e0253525. <http://doi.org/10.1371/journal.pone.0253525>.
17. C.G. Jiang, W. Wang, Q. Zhou, et al. Influence of age on the diagnostic accuracy of soluble biomarkers for tuberculous pleural effusion: a post hoc analysis. *BMC Pulm Med.* 2020; 20(1): 178. <http://doi.org/10.1186/s12890-020-01219-2>.
18. T.R. Tay, A. Tee. Factors affecting pleural fluid adenosine deaminase level and the implication on the diagnosis of tuberculous pleural effusion: a retrospective cohort study. *BMC Infect Dis.* 2013; 13: 546. <http://doi.org/10.1186/1471-2334-13-546>.
19. J.M. Porcel, M. Azzopardi, C.F. Koegelenberg, et al. The diagnosis of pleural effusions. *Expert Rev Respir Med.* 2015; 9(6): 801-15. <http://doi.org/10.1586/17476348.2015.1098535>.
20. E. Volpe, M. Sambucci, L. Battistini, G. Borsellino. Fas-Fas Ligand: Checkpoint of T Cell Functions in Multiple Sclerosis. *Front Immunol.* 2016; 7: 382. <http://doi.org/10.3389/fimmu.2016.00382>.
21. M. Lettau, M. Paulsen, D. Kabelitz, O. Janssen. Storage, expression and function of Fas ligand, the key death factor of immune cells. *Curr Med Chem.* 2008; 15(17): 1684-96. <http://doi.org/10.2174/092986708784872384>.
22. S.M. Mariani, B. Matiba, C. Bäuml, P.H. Krammer. Regulation of cell surface APO-1/Fas (CD95) ligand expression by metalloproteases. *Eur J Immunol.* 1995; 25(8): 2303-7. <http://doi.org/10.1002/eji.1830250828>.
23. P. Korczynski, J. Klimiuk, A. Safianowska, R. Krenke. Impact of age on the diagnostic yield of four different biomarkers of tuberculous pleural effusion. *Tuberculosis (Edinb).* 2019; 114:

- 24-9. <http://doi.org/10.1016/j.tube.2018.11.004>.
24. S.H. Wu, C.T. Li, C.H. Lin, et al. Soluble Fas ligand is another good diagnostic marker for tuberculous pleurisy. *Diagn Microbiol Infect Dis.* 2010; 68(4): 395-400. <http://doi.org/10.1016/j.diagmicrobio.2010.08.008>.

3. 拟开展研究课题的研究内容、研究目标、创新性和预期成果:

研究内容及技术路线

(1) 比

实

及

差

相

(2) 采用受试者工作特征(ROC)曲线法分析胸水中 sFasL 的诊断性能。在本部分研究中, 我

们

L

和

体

下

界

断

(PP

(3) 采用决策曲线法(DCA)分析胸水中 sFasL 和 ADA 为 TPE 患者带来的净受益。在本部分研究中, 我们主要利用 R 软件的 rmda 包绘制决策曲线, 分析两者为 TPE 患者带来的净受益。

(4) 研究血清和胸水中的 sFasL 能否带来增量诊断信息(added value)。在本部分研究中, 主

要

带来

增

白细

胞

旧模

型)

(命名

为

stic),

随

是否

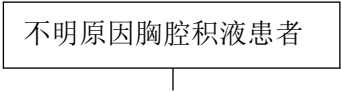
带来了增量诊断信息。

(5) 以列线图(nomogram)的形式将联合诊断结果进行可视化。在本部分研究中，主要是在小，

(6) 分析影响胸水 sFasL 诊断性能的因素。在本部分研究中，我们主要采用两种方法分析潜析年sL

诊断性能的因素。

技术路线：



研究目标

- (1) 阐
- (2) 明。
- (3) 探

创新性

本课题将采用前瞻性队列研究设计，通过多中心、大样本、长期随访，综合评价净受益。本研究采用的诊断性试验具有较高的敏感性和特异性，数据准确可靠。分析结果将结合临床实践，评估其临床应用价值和社会意义。

预期成果

预计在国际学术杂志上发表论文 1 篇。

三、拟开展本课题研究的现有基础：

- 已完成三篇相关课题的实验及论文的撰写：
- 1. Yan Z#, et al. (2020). Biomarker for the diagnosis of Meta-An. *Journal of Clinical Investigation*, 130(12), 3456-3465. (IF: 3.320)
 - 2. Yan Z#, et al. (2021). Diagnostic value of WQ. *Journal of Clinical Investigation*, 131(1), 1-10. (IF: 3.320)
 - 3. Yan Z#, et al. (2022). Diagnostic accuracy of WQ. *Journal of Clinical Investigation*, 132(1), 1-10. (IF: 3.320)

通过参与这些临床研究和 meta 分析，我熟练掌握了诊断实验设计和统计学分析要点，

腔积

Open

(呼和

因胸

京队

论更

。

科研计划到此截止

十.材料12.其他材料

- (1) 个人简历，中文格式化简历，限 1 页，含证件照；
- (2) 个人陈述，要求：用英文撰写，格式不限，可包括既往学习和研究经历，报考原因，学习计划等；
- (3) 社会活动与奖励，要求：个人特长，硕士期间参与的活动和受到的奖励，并注明其中承担的具体工作；
- (4) 清晰单人生活照一张，无修图。

(1) 个人简历

姓名		性别	女	出生年月	1994. 5	
政治面貌	党员	本人手机		应急电话		
本科院校		所学专业	生物技术			
硕士院校		所学专业	遗传学			
CET-4 成绩		CET-6 成绩		其它相关证书	国家计算机二级	
学习工作经历 (大学开始)	起止年月		学习和工作单位		任何职务	
	2013.9-2017.6				班长	
	2017.2-2017.6				实习生	
	2017.6-2020.9		中国人民解放军军事科学院 军事医学研究院		科研助理	
	2020.9-2023.6		信阳师范学院		无	
科研成果	1. ca 2. Ap 3. 药 4. Ep Ne 及					al 2 国 us e.
掌握的实验技能	熟练掌握基原代细胞培养、细胞转染、流式细胞术、免疫荧光、Western blot、RT-PCR、pull-down、分子对接、动物实验，并有蛋白质组测序生物信息学分析基础					
参与项目	1. 要工 2. 键技					主 关
获得荣誉	8000 元)					
硕士期间综合测评排名			2022-2023 学年： 1/17 2021-2022 学年： 6/17 2020-2021 学年： 7/17			

(2) 个人陈述

I g	ing in
biotec	many
school	t and
excelle	efore
pursui	y and
pharm	major
researc	r and
NLRP	eriod,
I am	metry,
immun	g and
animal	aster
degree	e won
first-cl	main
researc	from
proteo	as the
first a	been
submit	e and
improv	
Du	e and
practic	fields
deeply	to go
on for	
In	bining
transcr	brain
injury	tolide
against	
I'	ill be
long, I s a searc .	

(3) 社会活动与奖励，要求：个人特长，硕士期间参与的活动和受到的奖励，并注明其中承担的具体工作

无此文件

(4) 清晰生活照

